Analytic results for scalar-mediated Higgs boson production in association with two jets

OPEN ACCESS
IOP Publishing
Journal of Physics G: Nuclear and Particle Physics
J. Phys. G: Nucl. Part. Phys. **48** (2021) 085006 (35pp)
https://doi.org/10.1088/1361-6471/abf7d6

Analytic results for scalar-mediated Higgs boson production in association with two jets

Lucy Budge[1], John M Campbell[2], R Keith Ellis[1,*] and Satyajit Seth[3]

[1] Institute for Particle Physics Phenomenology, Durham University, Durham, DH1 3LE, United Kingdom
[2] Fermilab, PO Box 500, Batavia IL 60510-5011, United States of America
[3] Physical Research Laboratory, Navrangpura, Ahmedabad-380009, India

E-mail: lucy.budge@durham.ac.uk, johnmc@fnal.gov, keith.ellis@durham.ac.uk and seth@prl.res.in

Received 17 February 2021, revised 1 April 2021
Accepted for publication 14 April 2021
Published 8 July 2021

Abstract

We present compact analytic formulae for all one-loop amplitudes representing the production of a Higgs boson in association with two jets, mediated by a colour triplet scalar particle. Many of the integral coefficients present for scalar mediators are identical to the case when a massive fermion circulates in the loop, reflecting a close relationship between the two theories. The calculation is used to study Higgs boson production in association with two jets in a simplified supersymmetry (SUSY) scenario in which the dominant additional contributions arise from loops of top squarks. The results presented here facilitate an indirect search for top squarks in this channel, by a precision measurement of the corresponding cross section. However, we find that the potential for improved discrimination between the Standard Model and SUSY cases suggested by the pattern of results in the one- and two-jet samples is unlikely to be realized due to the loss in statistical power compared to an inclusive analysis.

Keywords: collider physics, Higgs boson, jets

(Some figures may appear in colour only in the online journal)

*Author to whom any correspondence should be addressed.

1. Introduction

The main production channel of Higgs bosons at the Large Hadron Collider (LHC) is through gluon–gluon fusion, i.e., $gg \to h$. The leading-order process starts at one loop, mediated by massive quark(s) of the Standard Model (SM). By marrying high-quality data from run 2 of the LHC with precision theoretical calculations for this process [1, 2], one can extract ever more exquisite determinations of the properties of the Higgs boson [3, 4].

As more data are collected, additional information can be obtained from analysing differential information beyond inclusive cross sections. One reason this is important is that additional jet activity allows new kinematic regions to be examined that may be more sensitive probes of Higgs properties. An example of this is that the nature of the Higgs coupling to particles circulating in the loop can only be probed if the relevant energy scale is at least of the order of the particle's mass. For inclusive production the relevant energy scale is the Higgs mass and, since $m_h < m_t$, one can describe this process using an effective field theory (EFT) in which the loop of heavy top quarks is replaced by an effective Lagrangian,

$$\mathcal{L}_{\text{eff}} = \frac{g_s^2}{48\pi^2 v}\, h\, G^A_{\mu\nu} G^{A,\mu\nu}, \tag{1.1}$$

where g_s is the strong coupling constant, v is the vacuum expectation value of the Higgs field, $G_{\mu\nu}$ is the QCD field strength, and h is the Higgs boson field. Indeed, the efficacy of this approximation is the very reason that such high-precision calculations of this process can be performed [1, 2]. In the presence of additional jet activity the relevant energy scale is no longer m_h but is instead the transverse momentum (p_T) of the leading jet. Therefore, the Higgs + jet process can become especially sensitive to the coupling of the Higgs boson to new mediator particles of mass m_X once $p_T > m_X$. An analysis of the cross section for this process, in this kinematic regime, could thus provide the first signal of new physics (in the case of a deviation from the SM prediction), or a stringent bound on the mass and coupling of any new mediator particle. Although less sensitive than corresponding direct searches, such indirect probes of the mediator particles are insensitive to any assumptions regarding the nature of their decay chains and may therefore provide complementary information.

Massive colour triplet scalar particles that arise in beyond the Standard Model (BSM) scenarios are potential new mediators for couplings of gluons to the Higgs boson. Indeed, one of the main goals of the LHC is to further explore the particles to which the Higgs boson couples, and having already discovered one fundamental scalar particle, it is natural to consider whether further scalar degrees of freedom might exist. One such proposed scalar particle is the top squark, a super partner of the SM top quark that appears in the Minimal Supersymmetric Standard Model (MSSM). The effect of such loops of particles has been explored previously [5–7], focussing on effects in either inclusive Higgs production or in the case of the Higgs boson recoiling against a single jet. Most recently, reference [8] demonstrated that the one-jet process offers, in principle, superior information to inclusive production over certain regions of parameter space. For the top squark, current indirect limits from Higgs and electroweak data [9, 10] are around $m_{\tilde{t}} \sim 300$ GeV. As noted above, this limit is clearly much weaker than any direct limit derived from a specific decay chain, which is currently around the 1 TeV scale (see, for example, references [11, 12] for recent limits from CMS and ATLAS).

In this paper we will extend this analysis to the case in which a Higgs boson is produced in association with two jets. To do so, we have performed a new calculation of the amplitudes for the scattering of a Higgs boson with four partons, mediated by a loop of colored scalar particles. Our results are expressed in the form of compact analytic expressions, exploiting a close correspondence with their fermionic counterparts [13]. The resulting expressions may

be evaluated numerically in a fast and stable manner, allowing for the construction of an efficient Monte Carlo event generator. We first outline the generic scalar theory in which we shall perform our calculation, as well as the specific MSSM case, in section 2. An overview of the computation of the four-parton matrix elements entering the Higgs + 2 jet analysis is given in section 3. The detailed results for one-loop integral coefficients for the case of a scalar loop are described in appendix A. We move to phenomenology in section 4, first providing a recalculation and recap of results for the zero- and one-jet cases before presenting our new two-jet analysis in section 5. Our conclusions are drawn in section 6. Finally, as an aid to performing an independent implementation of the formulae presented here, appendix B provides numerical results for the integral coefficients given in appendix A, and appendix C details the connection between our amplitudes and those obtained in the EFT.

2. Setup

We first formulate a generic scalar theory involving a complex scalar ϕ which carries $SU(3)$ colour in the triplet representation. The Lagrangian involving ϕ thus reads

$$\mathcal{L} = (D^\mu \phi_i^\dagger)(D_\mu \phi_i) - \lambda \phi_i^\dagger \phi_i h, \quad D_\mu \phi_i = \partial_\mu \phi_i + i \frac{g_s}{\sqrt{2}} (t \cdot \mathcal{G}_\mu)_{ij} \phi_j, \tag{2.1}$$

where $\mathcal{G}_\mu^a$ denotes the gluon field, t^a represents the standard $SU(3)$ colour generators, normalized such that $\mathrm{tr}(t^a t^b) = \delta^{ab}$, and g_s is the strong coupling constant. The coupling of the Higgs boson to the scalar field is denoted by the parameter λ.

2.1. Overview

In order to elucidate the differences and similarities between the cases of Higgs boson production mediated by a fermion and a scalar loop, we first examine the amplitudes for inclusive Higgs boson production via these two processes.

In the SM, where the particle in the loop is a quark of mass m, the amplitude for $g(p_1)g(p_2) \to h$ takes the following form:

$$\begin{aligned}\mathcal{H}_2^{gg} = i \frac{g_s^2}{16\pi^2} \delta^{AB} \left(\frac{m^2}{v}\right) \left[g^{\mu\nu} - \frac{p_1^\nu p_2^\mu}{p_1 . p_2}\right] \\ \times \left[(2m_h^2 - 8m^2) C_0(p_1, p_2; m) - 4\right] \epsilon_\mu(p_1) \epsilon_\nu(p_2).\end{aligned} \tag{2.2}$$

The gluons have colour labels A and B, ϵ represents a polarization vector, and m_h denotes the mass of the Higgs boson. The integral over the loop momentum is encapsulated in the scalar triangle function $C_0(p_1, p_2, m)$ defined later in equation (3.7). The corresponding result for a loop containing a scalar particle of mass m is [14]

$$\begin{aligned}\mathcal{A}_2^{gg} = i \frac{g_s^2}{16\pi^2} \delta^{AB} \left(\frac{-\lambda}{4}\right) \left[g^{\mu\nu} - \frac{p_1^\nu p_2^\mu}{p_1 . p_2}\right] \\ \times \left[-8m^2 C_0(p_1, p_2; m) - 4\right] \epsilon_\mu(p_1) \epsilon_\nu(p_2).\end{aligned} \tag{2.3}$$

Writing the amplitudes in this way highlights several similarities between them. When setting $(-\lambda/4) = m^2/v$ the coefficient of the triangle integral proportional to m^2 is identical, as well as the purely rational term (-4). This illustrates a general correspondence between such coefficients in the scalar and fermion theories [13].

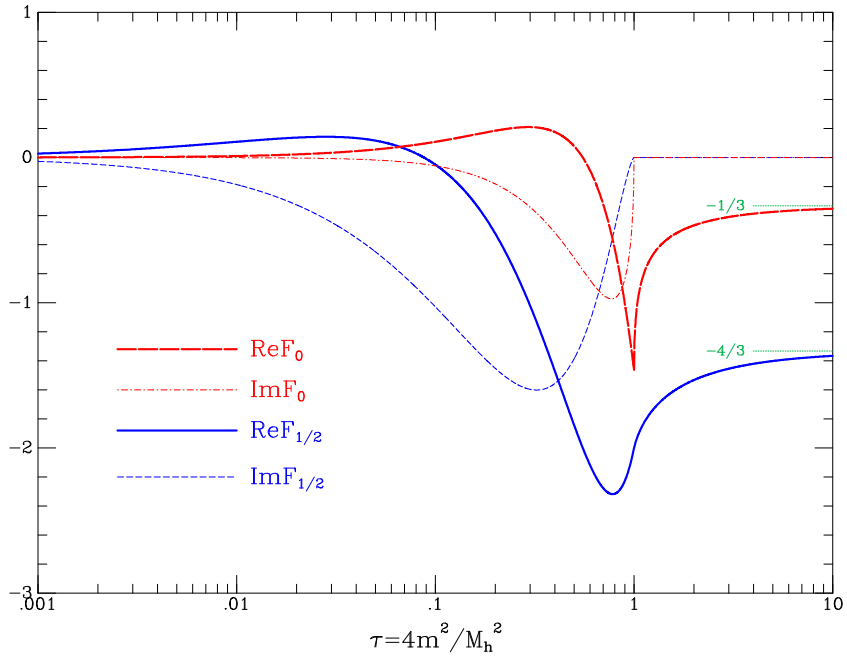

Figure 1. (in colour online) Functions $F_{1/2}$ and F_0, given in equations (2.5) and (2.6) respectively, plotted as a function of their arguments. The dotted lines show their asymptotes at large τ.

It is instructive to push this comparison further by extracting an overall factor as follows:

$$\mathcal{H}_2^{gg} = i\,\frac{g_s^2}{16\,\pi^2}\,\delta^{AB}\left[\frac{1}{2}\left(g^{\mu\nu} - \frac{p_1^\nu\, p_2^\mu}{p_1.p_2}\right)\right]\left(\frac{m_h^2}{v}\right)\epsilon_\mu(p_1)\epsilon_\nu(p_2)\,F_{1/2}(\tau),$$
$$\mathcal{A}_2^{gg} = i\,\frac{g_s^2}{16\,\pi^2}\,\delta^{AB}\left[\frac{1}{2}\left(g^{\mu\nu} - \frac{p_1^\nu\, p_2^\mu}{p_1.p_2}\right)\right]\left(\frac{\lambda}{2}\frac{m_h^2}{m^2}\right)\epsilon_\mu(p_1)\epsilon_\nu(p_2)\,F_0(\tau), \qquad (2.4)$$

where the functions for the scalar and fermionic cases are given by

$$F_0(\tau) = \tau\,[1 - \tau f(\tau)]\,, \qquad (2.5)$$
$$F_{1/2}(\tau) = -2\tau\,[1 + (1-\tau)f(\tau)]\,, \qquad F_{1/2}(\tau) = -2F_0(\tau) - 2\tau f(\tau), \qquad (2.6)$$

and $\tau = 4m^2/m_h^2$. In these formulae we have introduced the triangle function $f(\tau) = -\frac{m_h^2}{2}\,C_0(p_1, p_2; m)$, for which the explicit result is

$$f(\tau) = -\frac{1}{4}\theta(1-\tau)\left[\ln\left(\frac{1+\sqrt{1-\tau}}{1-\sqrt{1-\tau}}\right) - i\pi\right]^2 + \theta(\tau-1)\left[\sin^{-1}(1/\sqrt{\tau})\right]^2. \qquad (2.7)$$

Figure 1 shows the behaviour of F_0 and $F_{1/2}$ as a function of τ. In the region $\tau > 1$ the functions are both real and negative, and quickly approach their asymptotic values of $-1/3$ (scalar) and $-4/3$ (fermion). For the SM case $\tau \gg 1$ and the value of this function is in the asymptotic regime, motivating the use of the EFT shown in equation (1.1). From these asymptotic values and the overall factors extracted in equations (2.5) and (2.6) it is clear that the two processes

can be described by the same effective Lagrangian, in the limit of large intermediary mass, when we have $(\lambda/8) = m^2/v$.

2.2. Top squarks in the MSSM

Although the analytic results presented later in this paper are valid for a generic colour-triplet scalar, and may be applicable more generally, in this paper we will focus on the top squark sector of the MSSM, which contains two such scalars, $\tilde{t}_1$ and $\tilde{t}_2$. We will consider scenarios in which the coupling of the lightest Higgs boson in the MSSM is modified, assuming that this corresponds to the particle already observed at the LHC. Each squark couples to the lightest Higgs boson through a contribution to the Lagrangian of the form shown in equation (2.1), where we now label the strength of the Higgs coupling to each scalar by $\lambda_{h\tilde{t}_1\tilde{t}_1}$ and $\lambda_{h\tilde{t}_2\tilde{t}_2}$ respectively. Following reference [8], we parameterize this sector by

$$(m_{\tilde{t}_1}\ ,\ \Delta m\ ,\ \theta), \qquad \Delta m = \sqrt{m_{\tilde{t}_2}^2 - m_{\tilde{t}_1}^2}, \tag{2.8}$$

where, rather than using the two squark masses, we use the lightest top squark mass ($m_{\tilde{t}_1}$) and a measure of the separation with the other state (Δm). The final parameter (θ) is the mixing angle between the two scalar states, which takes values in the range $[-\pi/2, \pi/2]$. If the mass of the MSSM pseudoscalar (A) is much larger than the weak scale ($m_A \gg m_Z$) we can work in the decoupling limit [15], in which the Higgs–squark couplings take a very simple form:

$$\lambda_{h\tilde{t}_1\tilde{t}_1} = \frac{m_t^2}{v}\left(\alpha_1 \cos^2\theta + \alpha_2 \sin^2\theta + 2 - \frac{(\Delta m)^2}{2m_t^2}\sin^2 2\theta\right), \tag{2.9}$$

$$\lambda_{h\tilde{t}_2\tilde{t}_2} = \frac{m_t^2}{v}\left(\alpha_1 \sin^2\theta + \alpha_2 \cos^2\theta + 2 + \frac{(\Delta m)^2}{2m_t^2}\sin^2 2\theta\right). \tag{2.10}$$

The coefficients α_1 and α_2 in these formulae are given by

$$\alpha_1 = \frac{m_Z^2}{m_t^2}\cos 2\beta\left(1 - \frac{4}{3}\sin^2\theta_{\rm W}\right), \tag{2.11}$$

$$\alpha_2 = \frac{4}{3}\frac{m_Z^2}{m_t^2}\cos 2\beta \sin^2\theta_{\rm W}, \tag{2.12}$$

where $\theta_{\rm W}$ is the weak mixing angle. These formulae also contain the final MSSM parameter that is necessary to specify our model, β, where $\tan\beta$ is the ratio of the vacuum expectation value of the two Higgs bosons.

3. Calculation of Higgs + 2 jet process

We now provide the details of our calculation of the four-parton amplitudes that enter our analysis of the Higgs + 2 jet process.

3.1. Amplitudes for a scalar loop

We begin with the Lagrangian given in equation (2.1) and break the amplitude for the production of a Higgs boson and n gluons, mediated by a scalar loop, into colour-ordered sub-amplitudes. Following the notation of reference [13], we have

$$\mathcal{A}_n^{gggg}(\{p_i, h_i, c_i\}) = i\frac{g_s^n}{16\pi^2}\left(-\frac{\lambda}{4}\right)\sum_{\{1,2,\ldots,n\}'} \mathrm{tr}\,(t^{c_1}t^{c_2}\ldots t^{c_n})A_n^{\{c_i\}}(1^{h_1}, 2^{h_2}, \ldots n^{h_n}; h), \tag{3.1}$$

where the sum with the *prime*, $\sum_{\{1,2,\ldots,n\}'}$, is over all $(n-1)!$ *non-cyclic* permutations of $1,2,\ldots,n$, λ is the Higgs-scalar–scalar coupling and the t matrices are the SU(3) matrices in the fundamental representation normalized such that

$$\mathrm{tr}(t^a t^b) \;=\; \delta^{ab}. \tag{3.2}$$

m is the mass of the scalar circulating in the loop. It is sufficient to calculate one permutation in this sum, with the other colour sub-amplitudes related by Bose symmetry and obtained by exchange. The explicit result for the four-gluon case is

$$\begin{aligned}\mathcal{A}_4^{gggg}(\{p_i,h_i,c_i\}) \;=\; & i\frac{g_{\mathrm{s}}^4}{16\pi^2}\left(\frac{-\lambda}{4}\right)\Big\{\big[\mathrm{tr}\,(t^{c_1}t^{c_2}t^{c_3}t^{c_4}) \\ & + \mathrm{tr}\,(t^{c_1}t^{c_4}t^{c_3}t^{c_2})\big]\,A_4^{1234}(1^{h_1},2^{h_2},3^{h_3},4^{h_4};h) \\ & + \big[\mathrm{tr}\,(t^{c_1}t^{c_3}t^{c_4}t^{c_2}) + \mathrm{tr}\,(t^{c_1}t^{c_2}t^{c_4}t^{c_3})\big] \\ & \times A_4^{1342}(1^{h_1},2^{h_2},3^{h_3},4^{h_4};h) + \big[\mathrm{tr}\,(t^{c_1}t^{c_4}t^{c_2}t^{c_3}) \\ & + \mathrm{tr}\,(t^{c_1}t^{c_3}t^{c_2}t^{c_4})\big]\,A_4^{1423}(1^{h_1},2^{h_2},3^{h_3},4^{h_4};h)\Big\}. \end{aligned} \tag{3.3}$$

We also need the amplitude for the production of a Higgs boson, an antiquark, a quark and two gluons. It can be similarly decomposed into colour-ordered amplitudes as follows.

$$\begin{aligned}\mathcal{A}_4^{\bar{q}qgg}(\{p_i,h_i,c_i,j_i\}) = i\,\frac{g_{\mathrm{s}}^4}{16\pi^2}\left(\frac{-\lambda}{4}\right)\big[&(t^{c_3}\,t^{c_4})_{j_2\,j_1}A_4^{34}(1^{h_1},2^{-h_1},3^{h_3},4^{h_4};h) \\ & + (t^{c_4}\,t^{c_3})_{j_2\,j_1}A_4^{43}(1^{h_1},2^{-h_1},3^{h_3},4^{h_4};h)\big]. \end{aligned} \tag{3.4}$$

The colour structure $\delta^{c_3\,c_4}\,\delta_{j_2\,j_1}/N$ is also present in individual diagrams but makes no net contribution to the one-loop amplitude. Here we will give results for the colour-ordered amplitude A_4^{34} since it is straightforward to obtain A_4^{43} from this through the parity operation (complex conjugation) and permutation of momentum labels.

The four-quark amplitude takes the form

$$\mathcal{A}_4^{4q}(\{p_i,h_i,j_i\}) = i\,\frac{g_{\mathrm{s}}^4}{16\pi^2}\left(\frac{-\lambda}{4}\right)\,(t^{c_1})_{j_2\,j_1}\,(t^{c_1})_{j_4\,j_3}A_4^{4q}(1_{\bar{q}}^{h_1},2_q^{-h_1},3_{\bar{q}'}^{h_3},4_{q'}^{-h_3}), \tag{3.5}$$

where the helicities of the quarks are fixed by those of the antiquarks.

All colour subamplitudes are then decomposed in terms of scalar integrals. For instance, for the Higgs + 4 gluon case we have

$$\begin{aligned}A_4^{1234}(1^{h_1},2^{h_2},3^{h_3},4^{h_4};h) &= \frac{\bar{\mu}^{4-n}}{r_\Gamma}\frac{1}{i\pi^{n/2}}\int \mathrm{d}^n\,\ell\,\frac{\mathrm{Num}(\ell)}{\prod_i d_i(\ell)} \\ &= \sum_{i,j,k}\tilde{d}_{i\times j\times k}(1^{h_1},2^{h_2},3^{h_3},4^{h_4})\,D_0(p_i,p_j,p_k;m) \\ &\quad + \sum_{i,j}\tilde{c}_{i\times j}(1^{h_1},2^{h_2},3^{h_3},4^{h_4})\,C_0(p_i,p_j;m) \\ &\quad + \sum_i \tilde{b}_i(1^{h_1},2^{h_2},3^{h_3},4^{h_4})\,B_0(p_i;m) + \tilde{r}(1^{h_1},2^{h_2},3^{h_3},4^{h_4}). \end{aligned} \tag{3.6}$$

$\tilde{r}$ are the rational terms and the sums in the above equations scan over groupings of external gluons. The scalar bubble (B_0), triangle (C_0) and box (D_0) integrals are defined by

$$\begin{aligned}
B_0(p_1;m) &= \frac{\bar{\mu}^{4-n}}{r_\Gamma}\frac{1}{i\pi^{n/2}}\int \mathrm{d}^n\ell\,\frac{1}{D(\ell)D(\ell_1)},\\
C_0(p_1,p_2;m) &= \frac{1}{i\pi^2}\int \mathrm{d}^4\ell\,\frac{1}{D(\ell)D(\ell_1)D(\ell_{12})},\\
D_0(p_1,p_2,p_3;m) &= \frac{1}{i\pi^2}\int \mathrm{d}^4\ell\,\frac{1}{D(\ell)D(\ell_1)D(\ell_{12})D(\ell_{123})},\\
E_0(p_1,p_2,p_3,p_4;m) &= \frac{1}{i\pi^2}\int \mathrm{d}^4\ell\,\frac{1}{D(\ell)D(\ell_1)D(\ell_{12})D(\ell_{123})D(\ell_{1234})},
\end{aligned} \tag{3.7}$$

where the denominators are defined as

$$D(\ell) = \ell^2 - m^2 + i\varepsilon, \tag{3.8}$$

and the propagator momenta are

$$\begin{aligned}
\ell_1 &= \ell + p_1 = \ell + q_1,\\
\ell_{12} &= \ell + p_1 + p_2 = \ell + q_2,\\
\ell_{123} &= \ell + p_1 + p_2 + p_3 = \ell + q_3,\\
\ell_{1234} &= \ell + p_1 + p_2 + p_3 + p_4 = \ell + q_4.
\end{aligned} \tag{3.9}$$

Finally, $r_\Gamma = 1/\Gamma(1-\epsilon) + O(\epsilon^3)$ and $\bar{\mu}$ is an arbitrary mass scale.

As explained in reference [13], we have chosen to work in a basis without pentagon integrals. Nevertheless, we are left with some vestiges of their presence through pentagon-to-box reduction coefficients, $\mathcal{C}^{(i)}_{1\times2\times3\times4}$. These can be written as

$$\begin{aligned}
\mathcal{C}^{(1)}_{1\times2\times3\times4} &= -\frac{1}{2}\,\frac{s_{23}\,s_{34}\,[2\,s_{12}\,s_{24} + s_{13}\,s_{24} + s_{34}\,s_{12} - s_{23}\,s_{14}]}{16\;|S_{1\times2\times3\times4}|},\\
\mathcal{C}^{(2)}_{1\times2\times3\times4} &= -\frac{1}{2}\,\frac{s_{34}\,[s_{1234}\,s_{23}\,(s_{123} - 2\,s_{12}) + s_{123}\,(s_{34}\,(s_{123} - s_{23}) + s_{12}\,(s_{234} + s_{23}) - s_{234}\,s_{123})]}{16\;|S_{1\times2\times3\times4}|},\\
\mathcal{C}^{(3)}_{1\times2\times3\times4} &= -\frac{1}{2}\,\frac{[s_{14}\,s_{23} - (s_{12} + s_{13})\,(s_{24} + s_{34})]\,[s_{34}\,s_{12} + s_{23}\,s_{14} - s_{13}\,s_{24}]}{16\;|S_{1\times2\times3\times4}|},\\
\mathcal{C}^{(4)}_{1\times2\times3\times4} &= -\frac{1}{2}\,\frac{s_{12}\,[s_{1234}\,s_{23}\,(s_{234} - 2\,s_{34}) + s_{234}\,(s_{12}\,(s_{234} - s_{23}) + s_{34}\,(s_{123} + s_{23}) - s_{234}\,s_{123})]}{16\;|S_{1\times2\times3\times4}|},\\
\mathcal{C}^{(5)}_{1\times2\times3\times4} &= -\frac{1}{2}\,\frac{s_{12}\,s_{23}\,[2\,s_{34}\,s_{13} + s_{13}\,s_{24} + s_{34}\,s_{12} - s_{23}\,s_{14}]}{16\;|S_{1\times2\times3\times4}|}.
\end{aligned} \tag{3.10}$$

The denominator factor $|S_{1\times2\times3\times4}|$ is the determinant of the matrix $[S_{1\times2\times3\times4}]_{ij} = [m^2 - \frac{1}{2}(q_{i-1} - q_{j-1})^2]$, where q_i is the offset momentum; see equation (3.9). It is given by

$$\begin{aligned}
16\;|S_{1\times2\times3\times4}| &= s_{12}\,s_{23}\,s_{34}\;(s_{14}\,s_{23} - (s_{12} + s_{13})\,(s_{24} + s_{34})) + m^2\,G,\\
G &= (s_{12}\,s_{34} - s_{13}\,s_{24} - s_{14}\,s_{23})^2 - 4\,s_{13}\,s_{14}\,s_{23}\,s_{24}.
\end{aligned} \tag{3.11}$$

We use unitarity techniques to isolate the contributions of boxes [16], triangles [17] and bubbles [18–20]. Pentagon contributions to box coefficients are isolated by applying generalized unitarity cuts on five propagators in $d = (4 - 2\epsilon)$ dimensions, with subsequent modification as necessary to remove unphysical singularities and improve numerical stability [13]. The coefficients of each integral are subsequently simplified using the techniques of momentum twistors [21–24] and high precision floating-point arithmetic [25]. We exploit previous results obtained in the calculation of the same processes mediated by a fermion loop [13], noting that for our normalization the coefficients of bubble integrals, some triangle integrals, and the rational part are identical. The results of our analytic calculation of the amplitudes are presented in full in appendix A.

3.2. Squared matrix elements for fermion and scalar loops

With the scalar-mediated amplitude calculations in hand, we can now describe the calculation of the matrix elements relevant for the MSSM scenario described in section 2.2. For simplicity and practicality we will include only a top-quark loop in the SM calculation, although the inclusion of a bottom-quark loop is straightforward. We can write the subamplitude for an n-parton process mediated by the top quarks $\tilde{t}_1$ and $\tilde{t}_2$ as,

$$M_n^x = \left(\frac{m_t^2}{v}\right) H_n^x(m_t) - \left(\frac{\lambda_{h\tilde{t}_1\tilde{t}_1}}{4}\right) A_n^x(m_{\tilde{t}_1}) - \left(\frac{\lambda_{h\tilde{t}_2\tilde{t}_2}}{4}\right) A_n^x(m_{\tilde{t}_2}). \tag{3.12}$$

Note that we have taken care to label the mass dependence of the individual fermion and scalar subamplitudes, and this formula applies to any of the subamplitudes, e.g. $x = 1234$ $(gggg)$, $x = 34$ $(\bar{q}qgg)$ or $x = 4q$ $(\bar{q}q\bar{q}q)$. Expressions for all the relevant fermion-mediated subamplitudes H_n^x are given in reference [13].

We can now form the squared matrix elements used in our calculation. For the four-gluon case we can square the amplitude for a fixed helicity configuration and sum over colours to find

$$\begin{aligned}\sum_{\text{colours}} |\mathcal{M}_4^{gggg}|^2 = \left(\frac{g_s^4}{16\pi^2}\right)^2 (N^2-1)\Big\{2N^2\left(\left|M_4^{1234}\right|^2 + \left|M_4^{1342}\right|^2 + \left|M_4^{1423}\right|^2\right) \\ - 4\frac{(N^2-3)}{N^2}\left|M_4^{1234} + M_4^{1342} + M_4^{1423}\right|^2\Big\},\end{aligned} \tag{3.13}$$

where N is the dimensionality of the $SU(N)$ colour group, i.e. $N = 3$, and the labels for the helicity configuration (as explicitly shown in equation (3.3)) have been suppressed.

Squaring the $\bar{q}qgg$ amplitude and summing over colour yields,

$$\sum |\overset{\bar{q}qgg}{\underset{4}{\mathcal{M}}}|^2 = \left(\frac{g_s^4}{16\pi^2}\right)^2 (N^2-1)\left[N\left(|M_4^{34}|^2 + |M_4^{43}|^2\right) - \frac{1}{N}|M_4^{34} + M_4^{43}|^2\right], \tag{3.14}$$

where the labelling of the helicity configuration shown in equation (3.4) has again been suppressed.

Squaring and summing the four-quark amplitude over colours gives

$$\sum |\overset{4q}{\underset{4}{\mathcal{M}}}(h_1,h_3)|^2 = \left(\frac{g_s^4}{16\pi^2}\right)^2 (N^2-1)\,|M_4^{4q}(h_1,h_3)|^2, \tag{3.15}$$

when the quark lines have different flavours. For the case of identical quarks the sum over colours gives

$$\sum |\underset{4}{\overset{4q}{\mathcal{M}}}|^2 = \left(\frac{g_s^4}{16\pi^2}\right)^2 (N^2-1)\left(|M_4^{4q}(h_1,h_3)|^2 + |M_4^{4q'}(h_1,h_3)|^2 + \frac{\delta_{h_1h_3}}{N}\left(M_4^{4q}(h_1,h_3)M_4^{4q'}(h_1,h_3)^* + M_4^{4q}(h_1,h_3)^* M_4^{4q'}(h_1,h_3)\right)\right), \tag{3.16}$$

where, as indicated, the term on the second line only contributes for quarks of the same helicity and we have introduced

$$M_4^{4q'}(h_1,h_3) = M_4^{4q}(1_{\bar{q}}^{h_1}, 4_q^{-h_1}, 3_{\bar{q}}^{h_3}, 2_q^{-h_3}). \tag{3.17}$$

4. Recap of inclusive and one-jet results

In this section we briefly review results for the inclusive and one-jet cases, focussing on understanding the pattern of results observed in the existing literature.

For all the results presented in this paper we consider the LHC operating at $\sqrt{s} = 14$ TeV and employ the MMHT NLO set [26]. In addition, we use a choice of renormalization and factorization scales appropriate for the study of Higgs + multijet events,

$$\mu_f = \mu_r = \frac{H_T'}{2} = \frac{1}{2}\left(\sqrt{m_h^2 + p_{T,h}^2} + \sum_i |p_{T,i}|\right), \tag{4.1}$$

where the sum runs over any jets (equivalently, in our case, partons) present. The mass of the top quark is $m_t = 173.3$ GeV.

4.1. Inclusive cross section

From equation (2.4) we can abbreviate the form of the SM and simplified supersymmetry (SUSY) contributions to the amplitude for inclusive Higgs production as

$$\begin{aligned}\mathcal{M}^{\rm SM} &= \mathcal{H}_2^{gg} = C\,F_{1/2}(4m_t^2/m_h^2),\\ \mathcal{M}^{\rm SUSY} &= \mathcal{A}_2^{gg}(\tilde{t}_1) + \mathcal{A}_2^{gg}(\tilde{t}_2)\\ &= C\left[\left(\frac{v}{2m_{\tilde{t}_1}^2}\right)\lambda_{h\tilde{t}_1\tilde{t}_1}F_0(4m_{\tilde{t}_1}^2/m_h^2) + \left(\frac{v}{2m_{\tilde{t}_2}^2}\right)\lambda_{h\tilde{t}_2\tilde{t}_2}F_0(4m_{\tilde{t}_2}^2/m_h^2)\right],\end{aligned} \tag{4.2}$$

where C is a common overall factor that is unimportant for the following argument but which can be identified by comparison with equation (2.4). Since we are interested in measuring deviations from the SM result, it is useful to analyse the regions of SUSY parameter space in which these are expected to be small and therefore hard to probe. In order to simplify the argument we will make the simplifying assumption that we can always work in the EFT, i.e. that $m_t, m_{\tilde{t}_1}, m_{\tilde{t}_2} \gg m_h$, so that F_0 and $F_{1/2}$ can be replaced by their asymptotic values. This will be broadly true for the range of parameters in which we are interested but we note that, regardless, the features we elucidate here arise even when this no longer holds. Performing this replacement, we arrive at the simple result:

$$\mathcal{M}^{\rm SM} = -\frac{4C}{3}, \tag{4.3}$$

$$\mathcal{M}^{\rm SUSY} = -\frac{C}{3}\left[\left(\frac{v}{2m^2_{\tilde{t}_1}}\right)\lambda_{h\tilde{t}_1\tilde{t}_1} + \left(\frac{v}{2m^2_{\tilde{t}_2}}\right)\lambda_{h\tilde{t}_2\tilde{t}_2}\right]. \tag{4.4}$$

Since we are working in the limit in which the EFT is valid we can also drop the terms proportional to α_1 and α_2 (since they are suppressed by m_Z^2/m_t^2). In this case we have the further simplification of the SUSY amplitude:

$$\mathcal{M}^{\rm SUSY} = -\frac{C}{6}\left[\left(\frac{m_t^2}{m^2_{\tilde{t}_1}}\right)\left(2 - \frac{(\Delta m)^2}{2m_t^2}\sin^2 2\theta\right) + \left(\frac{m_t^2}{m^2_{\tilde{t}_2}}\right)\left(2 + \frac{(\Delta m)^2}{2m_t^2}\sin^2 2\theta\right)\right. \tag{4.5}$$

$$= -\frac{C}{3}\left[\frac{m_t^2}{m^2_{\tilde{t}_1}} + \frac{m_t^2}{m^2_{\tilde{t}_2}} - \frac{1}{4}\sin^2 2\theta\frac{(\Delta m)^4}{m^2_{\tilde{t}_1}m^2_{\tilde{t}_2}}\right], \tag{4.6}$$

cf equation (2.15) of reference [8].

The form of these amplitudes allows us to anticipate the situations when the SUSY contribution is very small. Due to the mixing allowed in the top-quark sector, this can occur when the SUSY amplitude itself vanishes. It is instructive to rewrite equation (4.6) as

$$\mathcal{M}^{\rm SUSY} = \frac{C}{12m^2_{\tilde{t}_1}m^2_{\tilde{t}_2}}\left[\sin^2 2\theta(\Delta m)^4 - 4m_t^2(\Delta m)^2 - 8m_t^2m^2_{\tilde{t}_1}\right], \tag{4.7}$$

so that the dependence on $m_{\tilde{t}_2}$ in the numerator has been eliminated. From this it is clear for which values of $m_{\tilde{t}_1}$, Δm and θ the amplitude vanishes, so that the SUSY result is very close to the SM one. Solving for $\mathcal{M}^{\rm SUSY} = 0$ we find this occurs when ($\theta > 0$)

$$\Delta m = m_t \times \sqrt{2} \times \sqrt{\frac{1 + \sqrt{1 + 2\sin^2 2\theta\, m^2_{\tilde{t}_1}/m_t^2}}{\sin^2 2\theta}}. \tag{4.8}$$

The coincidence of the SM and SUSY cross sections discussed above arises from a vanishing of the SUSY amplitude. In addition, there can be a further coincidence when the effect of interference between the SUSY and SM contributions cancels the contribution from the SUSY amplitude squared. In other words, we must have an alternative solution when

$$\begin{aligned}&\left(\mathcal{M}^{\rm SM} + \mathcal{M}^{\rm SUSY}\right)^2 - \left(\mathcal{M}^{\rm SM}\right)^2 = 0\\ &\Longrightarrow \mathcal{M}^{\rm SUSY} + 2\mathcal{M}^{\rm SM} = 0.\end{aligned} \tag{4.9}$$

Using the results in equations (4.3) and (4.6), we have

$$\mathcal{M}^{\rm SUSY} + 2\mathcal{M}^{\rm SM} = -\frac{C}{3}\left[\frac{m_t^2}{m^2_{\tilde{t}_1}} + \frac{m_t^2}{m^2_{\tilde{t}_2}} - \frac{1}{4}\sin^2 2\theta\frac{(\Delta m)^4}{m^2_{\tilde{t}_1}m^2_{\tilde{t}_2}} + 8\right]. \tag{4.10}$$

Manipulating as above, we find that this vanishes when

$$\sin^2 2\theta(\Delta m)^4 - 4(m_t^2 + 8m^2_{\tilde{t}_1})(\Delta m)^2 - 8m^2_{\tilde{t}_1}(m_t^2 + 4m^2_{\tilde{t}_1}) = 0. \tag{4.11}$$

This equation has no solutions for small Δm. On the other hand, for large Δm the SUSY and SM cross sections are identical when

$$\Delta m \approx 2\frac{\sqrt{m_t^2 + 8m^2_{\tilde{t}_1}}}{\sin 2\theta}. \tag{4.12}$$

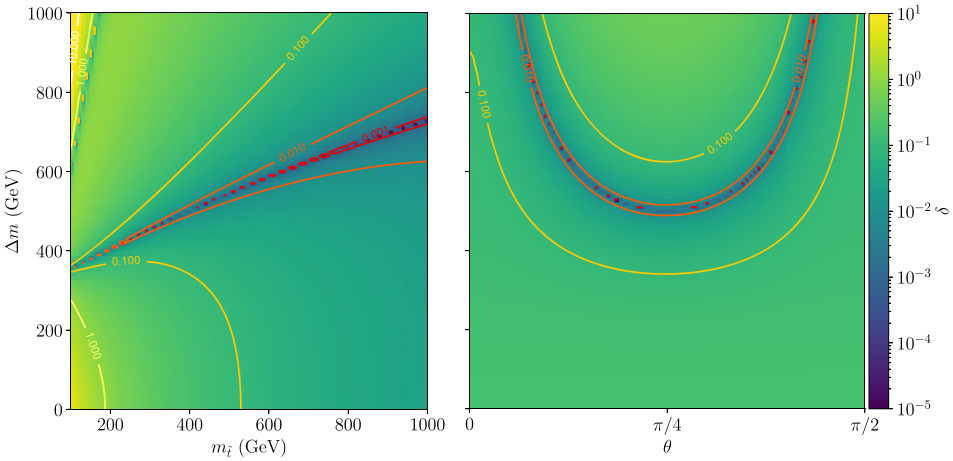

Figure 2. (in colour online) Deviation of the inclusive Higgs cross section from the SM case, measured by δ defined in equation (4.13). The left panel shows δ as a function of $m_{\tilde{t}_1}$ and Δm with top squarks mixing in a maximal fashion ($\theta = \frac{\pi}{4}$). In the right panel δ is shown as a function of θ and Δm, $m_{\tilde{t}_1} = 400$ GeV. In both panels $\tan\beta = 10$.

Again, this solution relies on the existence of a non-zero mixing ($\theta > 0$) between the squarks.

We now turn to a numerical study, measuring the deviation between the SUSY and SM cases by the quantity δ defined as [8]

$$\delta = \left| \frac{\sigma^{\mathrm{SM}} - \sigma^{\mathrm{SUSY}}}{\sigma^{\mathrm{SM}}} \right|. \tag{4.13}$$

As discussed above, the case of non-zero mixing is most interesting; in the absence of any mixing the SUSY contribution is simply additive. For this reason we focus on the case of maximal mixing ($\theta = \pi/4$) to illustrate the pattern of behaviour. Results for the case $\tan\beta = 10$, and as a function of the parameters $m_{\tilde{t}_1}$ and Δm, are shown in figure 2 (left). This figure demonstrates the regions of vanishing δ anticipated above. First, the vanishing of the SUSY amplitude occurs, in the maximal-mixing case, for values of Δm given by

$$\Delta m \approx m_t \sqrt{2\left(1 + \sqrt{2}\, m_{\tilde{t}_1}/m_t\right)}. \tag{4.14}$$

This corresponds to the dark blue stripe across the middle of the plot in figure 2 (left), already observed in reference [8]. The cancellation at the level of the cross section, i.e. as expected from equation (4.12), corresponds to the lighter blue line in the upper-left corner of the plot. In the region shown, $m_{\tilde{t}_1} \approx m_t$, it is approximately given by $\Delta m \approx 6 m_{\tilde{t}_1}$.

Note that, although we have used asymptotic results for the amplitudes to derive the presence and locations of the features above, these are clearly sufficient to capture the dominant effects. At smaller values of $m_{\tilde{t}_1}$, and to some extent Δm, the precise contours of vanishing δ vary slightly but are still present.

Although the maximal-mixing case is of highest interest here, as an indication of the effect of a smaller amount of mixing, figure 2 (right) shows similar contours as a function of θ and Δm, for fixed $m_{\tilde{t}_1} = 400$ GeV. Again the region of vanishing δ that is clearly visible in the figure is easily understood from equation (4.8).

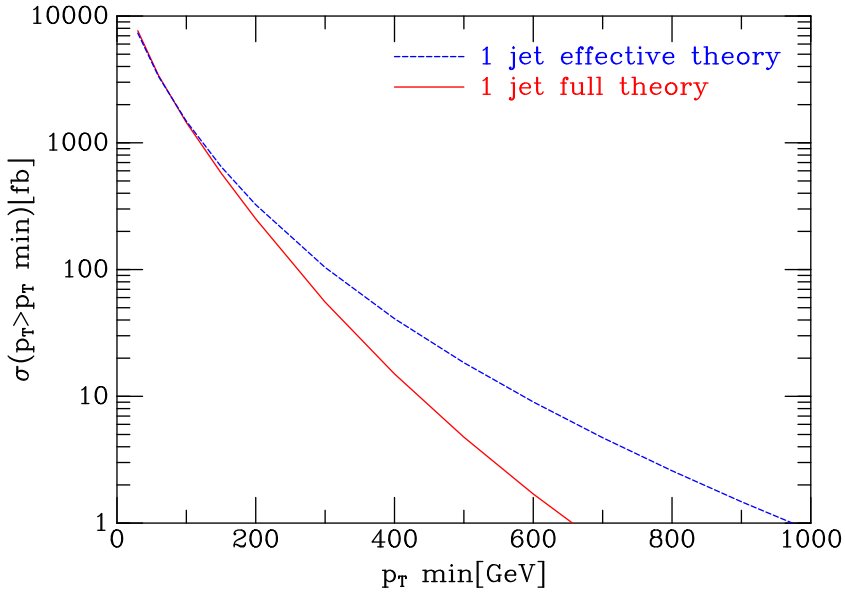

Figure 3. (in colour online) Lowest-order predictions for $H + 1$ jet in the SM model, computed in the EFT (dashed) and in the full theory (solid).

4.2. One-jet cross section

The case when the Higgs boson is produced in association with a jet has also been discussed extensively in the literature [6–8]. As explained in reference [8], the pattern of deviations from the SM is very similar to the inclusive case for low-p_T jets, but begins to differ as the jet (or equivalently, Higgs boson) is produced at large transverse momentum. A simple way to understand this behaviour is in terms of the ability of the jet to resolve the loop of coloured particles, which is demonstrated for the SM case in figure 3. To compute the cross sections shown in this figure we have defined jets according to a minimum p_T, also satisfying the requirement $|y(\text{jet})| < 2.4$. As discussed earlier, the calculations in the full theory and in the EFT only begin to differ around $p_T \sim 200$ GeV, i.e. when the jet is sufficiently energetic to resolve the top-quark loop. The same applies, of course, for the SUSY amplitude, except that the appropriate scales are now set by $m_{\tilde{t}_1}$ and Δm. In the low-p_T region both the SM and SUSY contributions to the amplitude can be computed in the effective theory and thus the pattern of deviations from the SM must be very similar to the inclusive case. Indeed, since the equality of the SM and SUSY cross sections is tied to the structure of the SUSY amplitude, the p_T of the jet should be of order $m_{\tilde{t}_1}$ in order to probe the dependence on the SUSY parameters more effectively.

This argument has been discussed in great detail in reference [8], from which we reproduce one set of results in order to illustrate this point. Figure 4 shows the dependence of δ on $m_{\tilde{t}}$ and Δm for the one-jet process, for two choices of minimum jet (Higgs) p_T. For the case of a low jet p_T cut, at 30 GeV (figure 4, left panel), the deviations from the SM case are essentially identical to the zero-jet case (cf figure 2, left). For a much higher cut, at 600 GeV, the jet is able to resolve at least the top quark loop and also the top squark, for values of $m_{\tilde{t}_1}$ up to a similar scale. This breaks the similarity with the zero-jet case, leading to larger deviations from the SM. This is most visible in the contours of constant δ, which are now more constraining for the one-jet case. This confirms the results presented in reference [8].

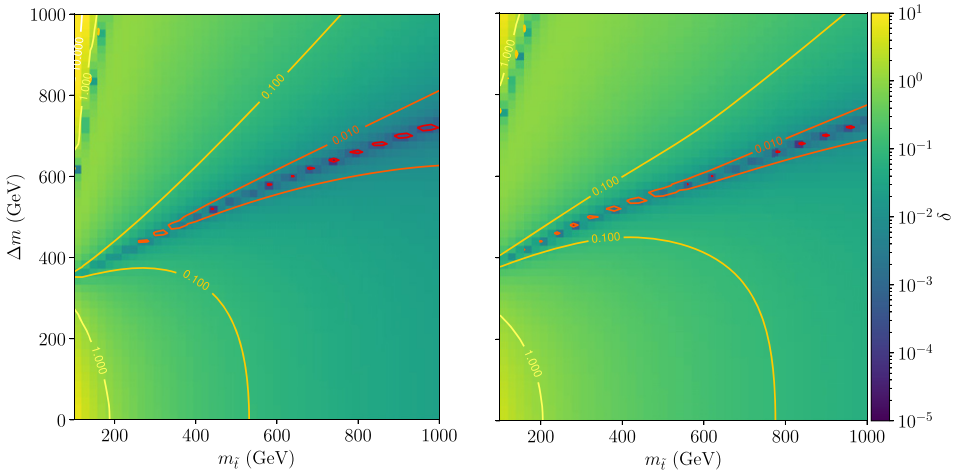

Figure 4. (in colour online) Deviation of the Higgs + 1 jet cross section from the SM case, measured by δ defined in equation (4.13), as a function of $m_{\tilde{t}_1}$ and Δm. Top squarks mix in a maximal fashion ($\theta = \frac{\pi}{4}$) and $\tan\beta = 10$. Results are shown for two choices of jet p_{T}: 30 GeV (left) and 600 GeV (right).

The region where the lightest top squark is degenerate with the top quark, $m_{\tilde{t}_1} \approx m_t$, has received considerable interest due to the difficulty of directly detecting a signal from such a model (see, for instance, reference [27] and references therein). Although in general this scenario results in large corrections to the Higgs boson rate, the blue lines in figure 2 (left) indicate the two regions where deviations are small and an indirect search via the inclusive Higgs cross section is similarly insensitive. However, applying a sufficiently high cut on the transverse momentum of the Higgs boson modifies both of these regions (figure 4, right) and such scenarios could be excluded by comparing the zero- and one-jet rates.

5. Results for the two-jet process

For the two-jet case we must supplement the jet p_{T} and rapidity threshold with a proper jet clustering algorithm. For this we choose the anti-k_{T} algorithm with a jet resolution parameter $R = 0.5$.

As we have already discussed, differences between the pattern of cross-section deviations are intimately connected to the breakdown of the EFT approach to describing these processes. We therefore first examine this for the two-jet case in the SM, with the results shown in figure 5. As the jet p_{T} cut is increased, the difference between the EFT and the full theory is not as pronounced in the two-jet case as in the one-jet process (comparing blue curves in figure 5 with figure 3). As explained in reference [28], which explored the limitations of the EFT by studying Higgs + 1, 2 and 3 jet processes, this is because the breakdown of the EFT is controlled by the p_{T} of the single hardest particle in the process. Requiring two very hard jets only serves to decrease the rate without providing an additional probe of the loop-induced Higgs coupling. Therefore, in order to drive the EFT breakdown more efficiently, and thus observe a different pattern of dependence on the SUSY parameters, we should employ a cut that requires a single hard particle. Therefore, we choose to cluster jets with the usual cut, $p_{\mathrm{T}}(\mathrm{jet}) > 30$ GeV, and then make a cut on the p_{T} of the Higgs boson. In this case the difference between the full theory and the EFT is very similar in the one- and two-jet cases (comparing

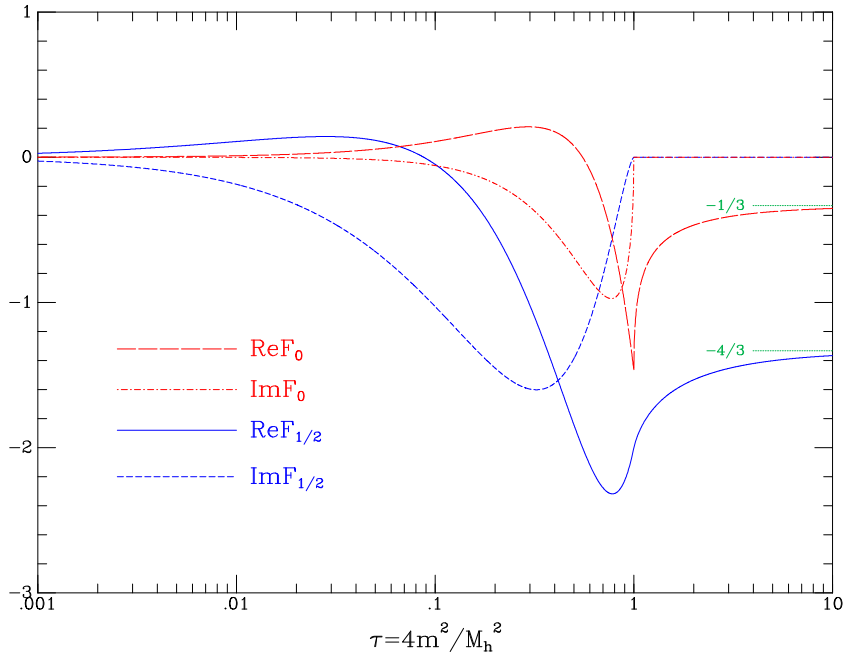

Figure 5. (in colour online) Rates for $H + 2$ jet production in the SM, as a function of a minimum p_{T}, computed in the full theory and EFT. Jets are either subject to this minimum p_{T} themselves (lower curves) or are only required to satisfy a 30 GeV cut and the minimum p_{T} cut is applied to the Higgs boson p_{T} (upper curves).

red curves in figure 5 with figure 3). We now use this same cut to explore the breakdown of the EFT for the case of a scalar particle in the loop, with results shown in figure 6. For this study we consider only the effect of a single scalar particle in the loop and no top quark, with the amplitudes for the scalar-mediated EFT implemented according to the discussion in appendix C. For a direct comparison with the fermion case, we show results for $m_{\mathrm{scalar}} = m_t = 173.3$ GeV, and also for a much higher mass, $m_{\mathrm{scalar}} = 600$ GeV. As expected, for each case the breakdown of the EFT occurs for $p_{\mathrm{T}}(H,\ \mathrm{min}) \sim m_{\mathrm{scalar}}$ [4].

As illustrated in figure 1, for the inclusive process, the behaviour of the fermionic and scalar amplitudes in the vicinity of the two-particle threshold differs. However, for the two-jet case, any such difference is not reflected at the level of the cross section, as shown in figure 7. Although the effective theory appears to work a little better for high $p_{\mathrm{T}}(\mathrm{min})$ in the scalar case, overall the two curves are very similar. In the limit of small $p_{\mathrm{T}}(\mathrm{min})$, the result in the full theory is actually larger than the one computed in the EFT in both cases. This is expected from the inclusive calculation, which these results should resemble as $p_{\mathrm{T}}(\mathrm{min}) \to 0$, where the ratios can be computed from equations (2.5) and (2.6) (cf also figure 1):

$$\sigma^{\mathrm{full}}(gg \to H)/\sigma^{\mathrm{EFT}}(gg \to H)|_{\mathrm{fermion}} = \left[F_{1/2}(4m_t^2/m_h^2)/(-4/3)\right]^2 = 1.065,$$

[4] Our choice of $m_{\mathrm{scalar}} = 600$ GeV is controlled by this fact. To investigate the effect of a heavy top squark at the LHC, we are limited to p_{T} ranges where one can accumulate sufficient statistics (see equation (5.2) below). The method in this paper has the advantage of being branching-ratio independent but, at the LHC, will not be able to investigate the $m_{\mathrm{scalar}} \approx 1$ TeV region probed by less inclusive methods [11, 12].

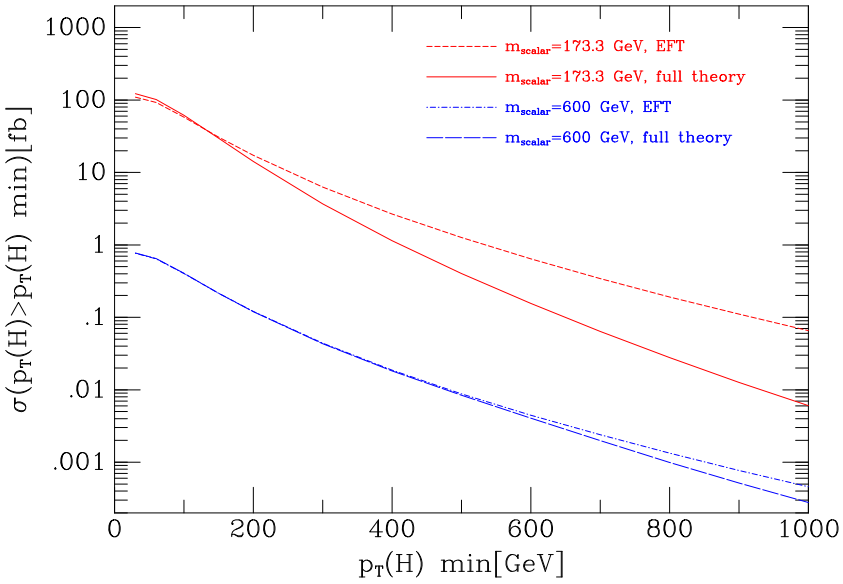

Figure 6. (in colour online) Rates for $H + 2$ jet production through a scalar loop, as a function of a minimum p_{T} applied to the Higgs boson, computed in the full theory and EFT. The scalar mediator mass is either 173.3 GeV (upper curves) or 600 GeV (lower curves).

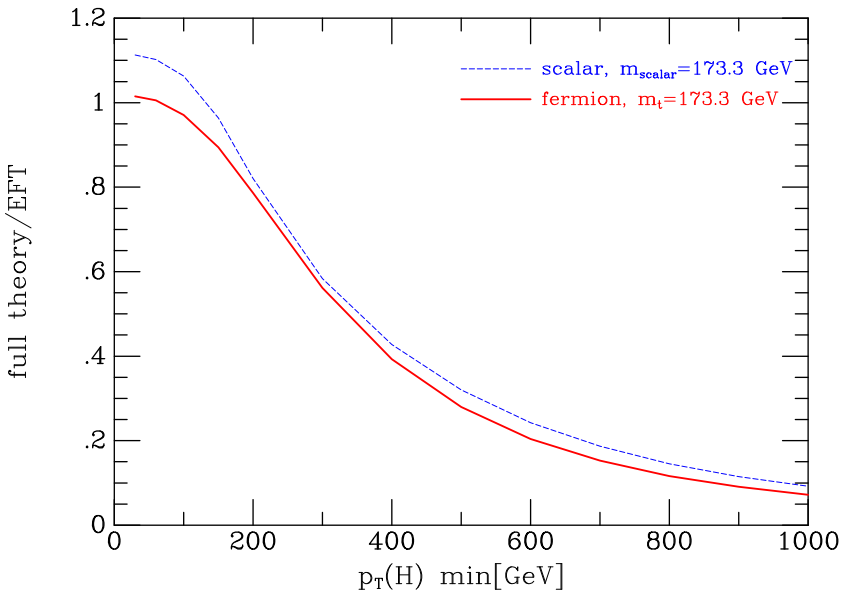

Figure 7. (in colour online) Ratio of the cross section in the full theory to that in the effective theory, for $H + 2$ jet production through a fermion (solid) and scalar (dashed) loop, as a function of a minimum p_{T} applied to the Higgs boson. The mass of the mediator is set to 173.3 GeV in both cases.

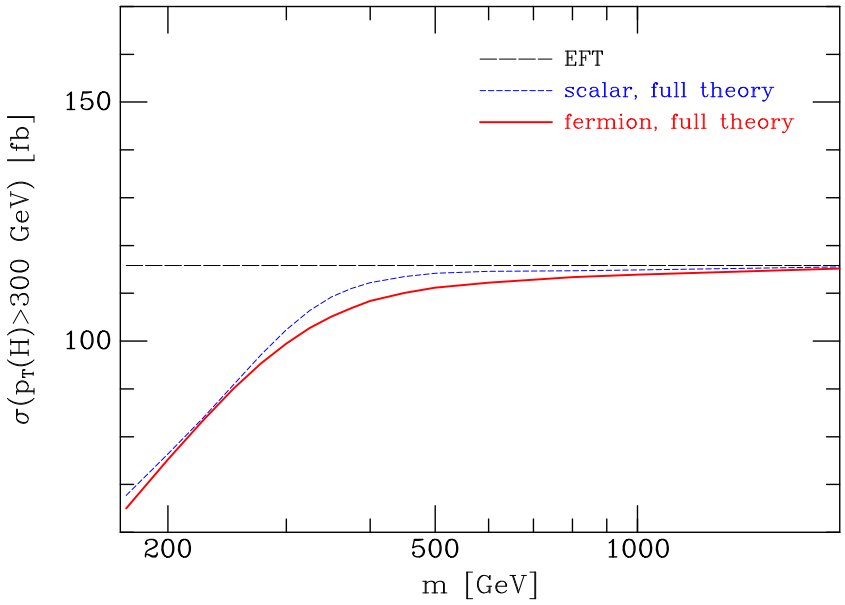

Figure 8. (in colour online) Cross section for $H + 2$ jet production through a fermion (solid) and scalar (dashed) loop, as a function of the mediator mass m, after application of a cut $p_{\mathrm{T}}(H) > 300$ GeV. The EFT result is shown as a horizontal dotted line.

$$\sigma^{\mathrm{full}}(gg \to H)/\sigma^{\mathrm{EFT}}(gg \to H)|_{\mathrm{scalar}} = \left[F_0(4m_t^2/m_h^2)/(-1/3)\right]^2 = 1.157. \tag{5.1}$$

Although the two curves in figure 7 never reach these values, due to the presence of the additional jets, they do reflect this underlying difference in the quality of the EFT. It should be stressed that, of course, in the limit of large mediator mass the effects of the loop can be described perfectly by the EFT. This is illustrated in figure 8, which shows the cross section for $p_{\mathrm{T}}(H) > 300$ GeV in the full theory, for both a fermion and a scalar mediator, as a function of the mediator mass, compared with the result in the EFT.

To examine the sensitivity of the two-jet process to the SUSY parameters, we again focus on the maximal-mixing case. We first assess the dependence on the minimum Higgs p_{T} cut that is applied, for the case of $m_{\tilde{t}_1} = 600$ GeV. The results are shown in figure 9. Note that we have covered a range of p_{T} that we expect to be accessible at the LHC—the cross section above 800 GeV is less than 0.5 fb, so around 1500 such Higgs events in the full HL–LHC dataset, $3ab^{-1}$. As indicated in the figure, the deviations are bigger in the two-jet case than for the inclusive cross section. However, the results are almost identical to the one-jet case; cf figure 2 of reference [8]. This is further reflected in the expected deviations from the SM shown in figure 10—a different pattern from the zero-jet process, but almost identical to the one-jet results shown in figure 4.

5.1. Discussion

In evaluating the discriminating power in the zero-, one- and two-jet cases above, we have focussed only on the deviations between the rates in the SM and SUSY cases. However, in order to observe such a difference, one must also take into account the number of events that could actually be produced in each case. Reading off the cross sections from figures 3 and 5 for

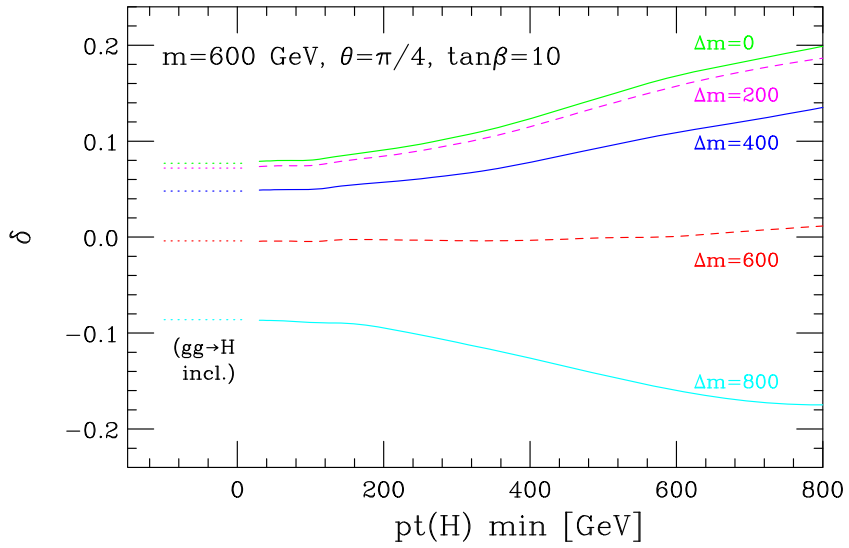

Figure 9. (in colour online) Two-jet calculation of δ (solid lines), as a function of the cut on the Higgs boson p_{T}, for the parameters $m_{\tilde{t}_1} = 600$ GeV, $\theta = \frac{\pi}{4}$ and $\tan\beta = 10$. The corresponding inclusive results are shown as dotted lines on the left of the figure.

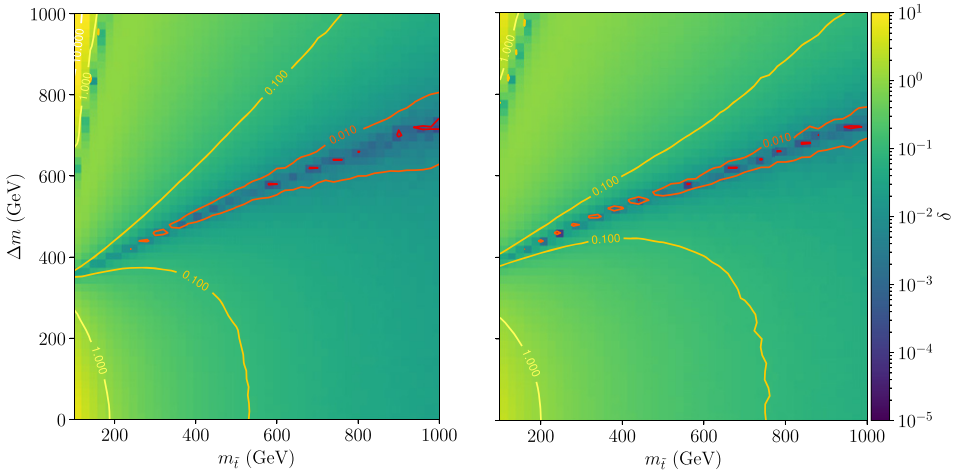

Figure 10. (in colour online) Deviation of the Higgs + 2 jet cross section from the SM case, measured by δ defined in equation (4.13), as a function of $m_{\tilde{t}_1}$ and Δm. Top squarks mix in a maximal fashion ($\theta = \frac{\pi}{4}$) and $\tan\beta = 10$. Results are shown in the cases of no additional cut (left) and $p_{\mathrm{T}}(H) > 600$ GeV (right).

$p_{\mathrm{T}}(\mathrm{jet}) > 30$ GeV, and using the (similarly leading-order) result for the inclusive cross section, we have

$$\sigma(gg \to H) = 18\,910 \text{ fb},$$
$$\sigma(gg \to H + 1 \text{ jet}) = 7640 \text{ fb},$$

$$\begin{aligned}\sigma(gg \to H + 2 \text{ jets}) &= 2230 \text{ fb}\,, \\ \sigma(gg \to H + 1 \text{ jet}) &= 2 \text{ fb} \qquad (p_{\mathrm{T}}(H) > 600 \text{ GeV}), \\ \sigma(gg \to H + 2 \text{ jets}) &= 2 \text{ fb} \qquad (p_{\mathrm{T}}(H) > 600 \text{ GeV}).\end{aligned} \tag{5.2}$$

Since the number of expected events with a highly boosted Higgs boson is so small, for both the one- and two-jet cases, it appears unlikely that the extra discriminating power could ever come into play. Even accounting for the fact that it may be possible to identify the $H \to b\bar{b}$ decay of the Higgs boson in the boosted case—essentially impossible for the bulk of Higgs boson events that occur at low p_{T}—the expected event sample would be at least two orders of magnitude smaller than any of the non-boosted ones. In such a case the improved discrimination between the SM and SUSY scenarios would never overcome the loss in statistical power. We note that this is not improved when considering an approximate inclusion of higher-order effects by rescaling these results by corrections computed in the EFT. The values of the K-factors in the EFT, defined by $K = \sigma^{\mathrm{NLO}}/\sigma^{\mathrm{LO}}$, are:

$$\begin{aligned}K(gg \to H) &= 1.91, \\ K(gg \to H + 1 \text{ jet}) &= 1.78\,, \\ K(gg \to H + 2 \text{ jets}) &= 1.72\,, \\ K(gg \to H + 1 \text{ jet}, p_{\mathrm{T}}(H) > 600 \text{ GeV}) &= 1.85, \\ K(gg \to H + 2 \text{ jets}, p_{\mathrm{T}}(H) > 600 \text{ GeV}) &= 1.42.\end{aligned} \tag{5.3}$$

Since the corrections become somewhat smaller as the jet multiplicity increases, in fact the expectation is that the statistical power becomes slightly poorer for the two-jet case compared to estimates based on the LO predictions shown in equation (5.2).

Of course, in making this argument we have neglected the role of systematic uncertainties. On the experimental side, the boosted configuration of the Higgs boson means that its decay products are more energetic and thus may be measured with smaller uncertainties. On the other hand, the precision of the SM theoretical prediction with which the data must be compared is much reduced, going from current percent-level uncertainties in an expansion up to $\mathrm{N^3LO}$ at the inclusive level [1, 2] to 10% level uncertainties from NNLO in the boosted case [29–33]. While it is clear that Higgs + multijet events offer a different handle on signals of new physics, a proper accounting of both statistical and systematic uncertainties is essential to fully understand their value.

6. Conclusions

In this paper we have provided an analytic calculation of all amplitudes representing the scattering of a Higgs boson and four partons, mediated by a loop of colour-triplet scalar particles.[5] By combining this with a previous calculation of the corresponding amplitudes in which the mediator particle is a fermion [13] we are able to describe modifications to the SM production of a Higgs boson in association with two jets in theories containing such scalar extensions. As an example we have analysed the specific case of the MSSM, which contains two relevant scalar particles, $\tilde{t}_1$ and $\tilde{t}_2$. Sensitivity to this scenario has previously been considered extensively

[5] A computer-readable form of all the integral coefficients presented in appendix A—which, together with the results in reference [13], is sufficient to reproduce these amplitudes—is provided at https://mcfm.fnal.gov/scalarcoeffs.tar.gz.

in the literature, for both inclusive production and the case of Higgs production in association with one jet. Our study is the first time such an analysis has been performed for the case of two jets.

The results of our calculation show that, although a two-jet analysis offers improved sensitivity compared to an inclusive analysis, it does not provide an additional benefit over the one-jet case. This can be understood by noting that, in order to probe the nature of the loop process most effectively, the two-jet analysis should demand only a single hard particle: either a jet or the Higgs boson itself. In either case the cross section is dominated by configurations in which the Higgs boson recoils against a single hard jet, with the second jet relatively soft. Such configurations are therefore one-jet-like, with the emission of the second jet well described by the QCD properties of soft and collinear factorization. Moreover, the loss in statistical power that ensues from selecting a sample of events in such a configuration cannot overcome the relatively small improvement in sensitivity. The same conclusion applies to studies of the one-jet rate at high transverse momentum.

Finally, we note that if a deviation from the SM prediction were observed in a sample of events containing Higgs bosons produced at high transverse momentum, it would be essential to have precision theoretical predictions for such configurations in a variety of BSM scenarios. The amplitudes presented in this paper are an ingredient in a next-to-leading order calculation of the Higgs + jet process in theories containing colour-triplet scalars.

Acknowledgments

We thank Giuseppe de Laurentis for his input and collaboration in the early stages of this project. The numerical calculations reported in this paper were performed using the Wilson High-Performance Computing Facility at Fermilab and the Vikram-100 High Performance Computing Cluster at the Physical Research Laboratory. This document was prepared using the resources of the Fermi National Accelerator Laboratory (Fermilab), a US Department of Energy, Office of Science, HEP User Facility. Fermilab is managed by Fermi Research Alliance, LLC (FRA), acting under Contract No. DE-AC02-07CH11359.

Data availability statement

The data that support the findings of this study are openly available at the following URL/DOI: mcfm.fnal.gov.

Appendix A. Four-parton integral coefficients for a scalar loop

In this section we provide expressions for all the box, triangle and bubble coefficients that can be treated as a minimal independent set for Higgs plus four-parton helicity amplitudes mediated by a massive scalar. For a complete description of the spinor notation, we refer the reader to [13]. Additional coefficients that can be obtained by momenta permutations and/or helicity flips are tabulated appropriately. As already noted, some of the coefficients are identical to the case when the circulating particle is a massive fermion [13]. Specifically, these are:

- The entire rational contribution, $\tilde{r}$.
- Bubble coefficients, $\tilde{b}_i$.
- A subset of triangle coefficients, $\tilde{c}_i$, where i labels all triangles where none of the external legs corresponds to the momentum of the Higgs boson.

- The m^2-dependent term in all triangle coefficients, $\tilde{c}_i^{(2)}$ (where, in general, we expand $\tilde{c}_i = \tilde{c}_i^{(0)} + \tilde{c}_i^{(2)} m^2$).

Expressions for such coefficients are not given here explicitly. Instead we refer to the equation numbers in reference [13] where they have already been reported. When the expressions for the whole coefficient coincide, these references are appended (inside brackets) in subsequent tables. For the partial coefficients, $\tilde{c}_i^{(2)}$, these references are included in the text.

As an aid to implementing these formulae in a numerical code, in appendix B we provide values for all of the coefficients provided here, when evaluated at a specific phase space point. We also give the numerical values of the finite parts of the full amplitudes, obtained by combining these coefficients with an evaluation of all loop integrals according to equation (3.6) (and its generalization to all partonic channels).

An additional check of the results presented here is that, in the limit of large mediator mass, all the amplitudes should match onto limiting forms obtained by an explicit calculation in the EFT. This equivalence is spelled out explicitly in appendix C.

A.1. Coefficients for $A_4^{1234}(g^+, g^+, g^+, g^+; h)$

For the case with four gluons of positive helicity, the complete result can easily be written in a form that includes a term proportional to the pentagon scalar integral (E_0):

$$\begin{aligned} A_4(h; 1_g^+, 2_g^+, 3_g^+, 4_g^+) = \Bigg[\Bigg\{ & \frac{4\,m^2}{\langle 1\,2\rangle\,\langle 2\,3\rangle\,\langle 3\,4\rangle\,\langle 4\,1\rangle} \\ & \times \Big[- tr_+\{1\,2\,3\,4\} m^2 E_0(p_1, p_2, p_3, p_4; m) \Big] \\ & + \frac{1}{2}((s_{12}+s_{13})(s_{24}+s_{34}) - s_{14}s_{23}) D_0(p_1, p_{23}, p_4; m) \\ & + \frac{1}{2} s_{12}s_{23} D_0(p_1, p_2, p_3; m) + (s_{12}+s_{13}+s_{14}) C_0(p_1, p_{234}; m) \\ & + 2\frac{s_{12}+s_{13}+s_{14}}{\langle 1\,2\rangle\,\langle 2\,3\rangle\,\langle 3\,4\rangle\,\langle 4\,1\rangle} \Bigg\} \\ & + \Big\{ 3 \text{ cyclic permutations} \Big\} \Bigg] . \end{aligned} \tag{A.1}$$

However, for consistency with the rest of our results and ease of implementation in a numerical code, we prefer to present this result in terms of only box, triangle and bubble coefficients. The box coefficients then take a very simple form when written in terms of the effective pentagon coefficient (obtained by calculating the pentagon coefficient in d dimensions and taking the $\mu^2 \to 0$ limit),

$$\tilde{e}_{1\times 2\times 3\times 4}(1^+, 2^+, 3^+, 4^+) = -4\,m^4 \frac{tr_+\{1\,2\,3\,4\}}{\langle 1\,2\rangle\,\langle 2\,3\rangle\,\langle 3\,4\rangle\,\langle 4\,1\rangle} = -4\,m^4 \frac{[1\,2]\,[3\,4]}{\langle 1\,2\rangle\,\langle 3\,4\rangle}. \tag{A.2}$$

The minimal set of integral coefficients needed to reconstruct the amplitude for this approach is given in the first and third columns of table 1.

A.1.1. $\tilde{d}_{1\times 2\times 34}$.

$$\tilde{d}_{1\times 2\times 34} = \mathcal{C}^{(4)}_{1\times 2\times 3\times 4}\, \tilde{e}_{\{1^+\times 2^+\times 3^+\times 4^+\}}. \tag{A.3}$$

Table 1. Minimal set of integral coefficients for $A_4^{1234}(g^+, g^+, g^+, g^+; h)$.

Coefficient	Related coefficients	Coefficient	Related coefficients
$\tilde{d}_{1\times2\times34}$	$\tilde{d}_{2\times3\times41}, \tilde{d}_{3\times4\times12}, \tilde{d}_{4\times1\times23}, \tilde{d}_{1\times4\times32}, \tilde{d}_{2\times1\times43}, \tilde{d}_{3\times2\times14}, \tilde{d}_{4\times3\times21}$	$\tilde{c}_{1\times234}$	$\tilde{c}_{2\times341}, \tilde{c}_{3\times412}, \tilde{c}_{4\times123}$
$\tilde{d}_{1\times23\times4}$	$\tilde{d}_{2\times34\times1}, \tilde{d}_{3\times41\times2}, \tilde{d}_{4\times12\times3}$		
$\tilde{d}_{1\times2\times3}$	$\tilde{d}_{2\times3\times4}, \tilde{d}_{3\times4\times1}, \tilde{d}_{4\times1\times2}$		

A.1.2. $\tilde{d}_{1\times23\times4}$.

$$\tilde{d}_{1\times23\times4}(1^+, 2^+, 3^+, 4^+) = C^{(3)}_{1\times2\times3\times4}\,\tilde{e}_{\{1^+\times2^+\times3^+\times4^+\}} + \frac{2\,m^2}{\langle1\,2\rangle\,\langle2\,3\rangle\,\langle3\,4\rangle\,\langle4\,1\rangle} \times [(s_{12}+s_{13})\,(s_{24}+s_{34}) - s_{14}\,s_{23}]. \tag{A.4}$$

A.1.3. $\tilde{d}_{1\times2\times3}$.

$$\tilde{d}_{1\times2\times3} = C^{(1)}_{4\times1\times2\times3}\,\tilde{e}_{\{4^+\times1^+\times2^+\times3^+\}} + C^{(5)}_{1\times2\times3\times4}\,\tilde{e}_{\{1^+\times2^+\times3^+\times4^+\}} + \frac{2\,m^2}{\langle1\,2\rangle\,\langle2\,3\rangle\,\langle3\,4\rangle\,\langle4\,1\rangle}\,s_{12}\,s_{23}. \tag{A.5}$$

A.1.4. $\tilde{c}^{(0)}_{1\times234}$, $\tilde{c}^{(2)}_{1\times234}$.

$$\tilde{c}^{(0)}_{1\times234}(1^+, 2^+, 3^+, 4^+) = 0. \tag{A.6}$$

We have $\tilde{c}^{(2)}_{1\times234}(1^+, 2^+, 3^+, 4^+) = c^{(2)}_{1\times234}(1^+, 2^+, 3^+, 4^+)$ where the fermionic coefficient is given in equation (4.10) of reference [13].

A.2. Coefficients for $A_4^{1234}(g^+, g^+, g^+, g^-; h)$

The effective pentagon coefficients [13] used to define the box coefficients below are

$$\tilde{e}_{\{1^+\times2^+\times3^+\times4^-\}} = -4\,m^4\,\frac{[2\,3]\;\langle4|(2+3)|1]}{\langle2\,3\rangle\;\langle1|(2+3)|4]}, \tag{A.7}$$

$$\tilde{e}_{\{4^-\times1^+\times2^+\times3^+\}} = \tilde{e}_{\{1^+\times2^+\times3^+\times4^-\}}\{1 \leftrightarrow 3\}, \tag{A.8}$$

$$\tilde{e}_{\{2^+\times3^+\times4^-\times1^+\}} = -4\,m^4\,\frac{[2\,3]^2\,\langle3\,4\rangle\,\langle2|(3+4)|1]}{\langle2\,3\rangle^2\,[3\,4]\,\langle1|(3+4)|2]}, \tag{A.9}$$

$$\tilde{e}_{\{3^+\times4^-\times1^+\times2^+\}} = \tilde{e}_{\{2^+\times3^+\times4^-\times1^+\}}\{1 \leftrightarrow 3\}. \tag{A.10}$$

The minimal set of integral coefficients needed to reconstruct the amplitude for this approach is given in the first and third columns of table 2.

Table 2. Minimal set of integral coefficients for $A_4^{1234}(g^+, g^+, g^+, g^-; h)$. The equation numbers in brackets give the places in reference [13] where the coefficients are reported. These coefficients are the same in the scalar-mediated and fermion-mediated theories.

Coefficient	Related coefficients	Coefficient	Related coefficients
$\tilde{d}_{1\times2\times34}$	$\tilde{d}_{3\times2\times14}$	$\tilde{c}_{3\times4}$ (5.19)	$\tilde{c}_{4\times1}$
$\tilde{d}_{1\times4\times32}$	$\tilde{d}_{3\times4\times12}$	$\tilde{c}_{2\times34}$ (5.20)	$\tilde{c}_{2\times14}$
$\tilde{d}_{2\times1\times43}$	$\tilde{d}_{2\times3\times41}$	$\tilde{c}_{1\times43}$ (5.21)	$\tilde{c}_{3\times41}$
$\tilde{d}_{4\times3\times21}$	$\tilde{d}_{4\times1\times23}$	$\tilde{c}_{4\times123}$	
$\tilde{d}_{2\times34\times1}$	$\tilde{d}_{3\times41\times2}$	$\tilde{c}_{1\times234}$	$\tilde{c}_{3\times412}$
$\tilde{d}_{1\times23\times4}$	$\tilde{d}_{4\times12\times3}$	$\tilde{c}_{2\times341}$	
$\tilde{d}_{2\times3\times4}$	$\tilde{d}_{4\times1\times2}$	$\tilde{c}_{12\times34}$	$\tilde{c}_{23\times41}$
$\tilde{d}_{1\times2\times3}$		$\tilde{b}_{34}$ (5.30)	$\tilde{b}_{14}$
$\tilde{d}_{3\times4\times1}$		$\tilde{b}_{234}$ (5.31)	$\tilde{b}_{412}, \tilde{b}_{341}$
		$\tilde{b}_{1234}$ (5.32)	

A.2.1. $\tilde{d}_{1\times2\times34}$.

$$\begin{aligned}\tilde{d}_{1\times2\times34}(1^+,2^+,3^+,4^-) = {} & \mathcal{C}^{(4)}_{1\times2\times3\times4}\,\tilde{e}_{\{1^+\times2^+\times3^+\times4^-\}} \\ & - 2\,m^2\frac{[1\,2]}{\langle1\,2\rangle}\left[\frac{\langle2\,4\rangle^2\ \langle4|(2+3)|1]}{\langle2\,3\rangle\ \langle3\,4\rangle\ \langle2|(3+4)|1]}\right. \\ & \left. + \frac{[2\,3]\ \langle1|(2+4)|3]^2}{[3\,4]\ \langle1|(3+4)|2]\ \langle1|(2+3)|4]}\right].\end{aligned} \tag{A.11}$$

A.2.2. $\tilde{d}_{1\times4\times32}$.

$$\begin{aligned}\tilde{d}_{1\times4\times32}(1^+,2^+,3^+,4^-) = {} & \mathcal{C}^{(2)}_{2\times3\times4\times1}\,\tilde{e}_{\{2^+\times3^+\times4^-\times1^+\}} \\ & + 2\,m^2\frac{[2\,3]\,s_{14}s^2_{234}}{\langle2\,3\rangle^2\,[3\,4]\,\langle1|(3+4)|2]\,\langle1|(2+3)|4]}.\end{aligned} \tag{A.12}$$

A.2.3. $\tilde{d}_{2\times1\times43}$.

$$\begin{aligned}\tilde{d}_{2\times1\times43}(1^+,2^+,3^+,4^-) = {} & \mathcal{C}^{(2)}_{3\times4\times1\times2}\,\tilde{e}_{\{3^+\times4^-\times1^+\times2^+\}} \\ & + 2\,m^2\frac{[1\,2]}{\langle1\,2\rangle}\left[\frac{[1\,3]^2\ \langle2|(1+4)|3]}{[1\,4]\ [3\,4]\ \langle2|(3+4)|1]}\right. \\ & \left. + \frac{\langle1\,4\rangle\ \langle4|(1+3)|2]^2}{\langle3\,4\rangle\ \langle1|(3+4)|2]\ \langle3|(1+4)|2]}\right].\end{aligned} \tag{A.13}$$

A.2.4. $\tilde{d}_{4\times3\times21}$.

$$\begin{aligned}\tilde{d}_{4\times3\times21}(1^+,2^+,3^+,4^-) = {} & \mathcal{C}^{(2)}_{1\times2\times3\times4}\,\tilde{e}_{\{1^+\times2^+\times3^+\times4^-\}} \\ & + 2\,m^2\frac{s_{34}\,s^2_{123}}{\langle1\,2\rangle\ \langle2\,3\rangle\ \langle1|(2+3)|4]\ \langle3|(1+2)|4]}.\end{aligned} \tag{A.14}$$

A.2.5. $\tilde{d}_{1\times 23\times 4}$.

$$\tilde{d}_{1\times 23\times 4}(1^+,2^+,3^+,4^-) = \mathcal{C}^{(3)}_{1\times 2\times 3\times 4}\,\tilde{e}_{\{1^+\times 2^+\times 3^+\times 4^-\}}. \tag{A.15}$$

A.2.6. $\tilde{d}_{2\times 34\times 1}$.

$$\begin{aligned}\tilde{d}_{2\times 34\times 1}(1^+,2^+,3^+,4^-) = \mathcal{C}^{(3)}_{2\times 3\times 4\times 1}\,\tilde{e}_{\{2^+\times 3^+\times 4^-\times 1^+\}} \\ + \frac{2\,\langle 2\,4\rangle}{\langle 1\,2\rangle\,\langle 2\,3\rangle}\left[\frac{\langle 1\,4\rangle\,\langle 2\,4\rangle\,\langle 1|(3+4)|2]\,\langle 2|(3+4)|1]}{\langle 1\,2\rangle^2\,\langle 3\,4\rangle}\right. \\ \left. - m^2\left(3\,\frac{\langle 1\,4\rangle\,\langle 2\,4\rangle\,[1\,2]}{\langle 1\,2\rangle\,\langle 3\,4\rangle} + 2\frac{[1\,3]\,[2\,3]}{[3\,4]} + \frac{\langle 2\,4\rangle\,[1\,4]\,[2\,3]}{\langle 2\,3\rangle\,[3\,4]}\right)\right].\end{aligned} \tag{A.16}$$

A.2.7. $\tilde{d}_{2\times 3\times 4}$.

$$\begin{aligned}\tilde{d}_{2\times 3\times 4}(1^+,2^+,3^+,4^-) = \mathcal{C}^{(1)}_{1\times 2\times 3\times 4}\,\tilde{e}_{\{1^+\times 2^+\times 3^+\times 4^-\}} \\ + \mathcal{C}^{(5)}_{2\times 3\times 4\times 1}\,\tilde{e}_{\{2^+\times 3^+\times 4^-\times 1^+\}} \\ + 2\,m^2\frac{s_{234}\,\langle 3\,4\rangle\,[2\,3]^2}{\langle 2\,3\rangle\,\langle 1|(3+4)|2]\,\langle 1|(2+3)|4]}.\end{aligned} \tag{A.17}$$

A.2.8. $\tilde{d}_{1\times 2\times 3}$.

$$\begin{aligned}\tilde{d}_{1\times 2\times 3}(1^+,2^+,3^+,4^-) = \mathcal{C}^{(5)}_{1\times 2\times 3\times 4}\,\tilde{e}_{\{1^+\times 2^+\times 3^+\times 4^-\}} \\ + \mathcal{C}^{(1)}_{4\times 1\times 2\times 3}\,\tilde{e}_{\{4^-\times 1^+\times 2^+\times 3^+\}} \\ + 2\,m^2\frac{s_{123}\,[1\,2]\,[2\,3]}{\langle 3|(1+2)|4]\,\langle 1|(2+3)|4]}.\end{aligned} \tag{A.18}$$

A.2.9. $\tilde{d}_{3\times 4\times 1}$.

$$\begin{aligned}\tilde{d}_{3\times 4\times 1}(1^+,2^+,3^+,4^-) = \mathcal{C}^{(1)}_{2\times 3\times 4\times 1}\,\tilde{e}_{\{2^+\times 3^+\times 4^-\times 1^+\}} + \mathcal{C}^{(5)}_{3\times 4\times 1\times 2}\,\tilde{e}_{\{3^+\times 4^-\times 1^+\times 2^+\}} \\ - 2m^2\frac{1}{\langle 1\,3\rangle}\left[\frac{[2\,3]\,\langle 3\,4\rangle^2\,s_{14}}{\langle 2\,3\rangle^2\,\langle 1|(3+4)|2]} + \frac{[1\,2]\,\langle 1\,4\rangle^2\,s_{34}}{\langle 1\,2\rangle^2\,\langle 3|(1+4)|2]}\right] \\ + \frac{\langle 1\,4\rangle\,\langle 3\,4\rangle}{\langle 1\,2\rangle\,\langle 1\,3\rangle^2\,\langle 2\,3\rangle}\left[2\,s_{14}\,s_{34} + 6\,m^2\,s_{13}\right].\end{aligned} \tag{A.19}$$

A.2.10. $\tilde{c}^{(0)}_{4\times123}$, $\tilde{c}^{(2)}_{4\times123}$.

$$\tilde{c}^{(0)}_{4\times123}(1^+,2^+,3^+,4^-) = 0. \tag{A.20}$$

We have $\tilde{c}^{(2)}_{4\times123}(1^+,2^+,3^+,4^-) = c^{(2)}_{4\times123}(1^+,2^+,3^+,4^-)$, where the fermionic coefficient is given in equation (5.23) of reference [13].

A.2.11. $\tilde{c}^{(0)}_{1\times234}$, $\tilde{c}^{(2)}_{1\times234}$.

$$\tilde{c}^{(0)}_{1\times234}(1^+,2^+,3^+,4^-) = 2(s_{12}+s_{13}+s_{14})\frac{\langle 1\,4\rangle\ \langle 2\,4\rangle^2}{\langle 1\,2\rangle^3\ \langle 2\,3\rangle\ \langle 3\,4\rangle}. \tag{A.21}$$

Moreover, we have $\tilde{c}^{(2)}_{1\times234}(1^+,2^+,3^+,4^-) = c^{(2)}_{1\times234}(1^+,2^+,3^+,4^-)$, where the fermionic coefficient is given in equation (5.25) of reference [13].

A.2.12. $\tilde{c}^{(0)}_{2\times341}$, $\tilde{c}^{(2)}_{2\times341}$.

$$\tilde{c}^{(0)}_{2\times341}(1^+,2^+,3^+,4^-) = 2(s_{12}+s_{23}+s_{24})\,\langle 2\,4\rangle^2\,\frac{\langle 1\,4\rangle^2\,\langle 2\,3\rangle^2+\langle 1\,2\rangle^2\,\langle 3\,4\rangle^2}{\langle 1\,2\rangle^3\,\langle 2\,3\rangle^3\ \langle 1\,4\rangle\ \langle 3\,4\rangle}. \tag{A.22}$$

Furthermore, $\tilde{c}^{(2)}_{2\times341}(1^+,2^+,3^+,4^-) = c^{(2)}_{2\times341}(1^+,2^+,3^+,4^-)$, where the fermionic coefficient is given in equation (5.27) of reference [13].

A.2.13. $\tilde{c}^{(0)}_{12\times34}$, $\tilde{c}^{(2)}_{12\times34}$.

$$\tilde{c}^{(0)}_{12\times34}(1^+,2^+,3^+,4^-) = 0. \tag{A.23}$$

In addition, $\tilde{c}^{(2)}_{12\times34}(1^+,2^+,3^+,4^-) = c^{(2)}_{12\times34}(1^+,2^+,3^+,4^-)$, where the fermionic coefficient is given in equation (5.29) of reference [13].

A.3. Coefficients for $A_4^{1234}(g^+,g^-,g^+,g^-;h)$

The effective pentagon coefficients for this helicity combination are

$$\tilde{e}_{\{1^+\times2^-\times3^+\times4^-\}} = -4m^4\frac{\langle 1\,2\rangle\,[3\,4]\,\langle 4|(2+3)|1]^2}{[1\,2]\,\langle 3\,4\rangle\,\langle 1|(2+3)|4]^2}, \tag{A.24}$$

$$\tilde{e}_{\{3^+\times4^-\times1^+\times2^-\}} = \tilde{e}_{\{1^+\times2^-\times3^+\times4^-\}}\,\{1\leftrightarrow3,\,2\leftrightarrow4\}, \tag{A.25}$$

$$\tilde{e}_{\{4^-\times1^+\times2^-\times3^+\}} = \tilde{e}_{\{1^+\times2^-\times3^+\times4^-\}}\,\{1\to4,\,2\to1,\,3\to2,\,4\to3,\,\langle\rangle\leftrightarrow[]\}, \tag{A.26}$$

$$\tilde{e}_{\{2^-\times3^+\times4^-\times1^+\}} = \tilde{e}_{\{1^+\times2^-\times3^+\times4^-\}}\,\{1\to2,\,2\to3,\,3\to4,\,4\to1,\,\langle\rangle\leftrightarrow[]\}. \tag{A.27}$$

The minimal set of coefficients that needs to be calculated is given in table 3.

Table 3. Minimal set of integral coefficients for $A_4^{1234}(g^+, g^-, g^+, g^-; h)$. The equation numbers in brackets give the places in reference [13] where the coefficients are reported. These coefficients are the same in the scalar-mediated and fermion-mediated theories.

Coefficient	Related coefficients	Coefficient	Related coefficients
$\tilde{d}_{4\times3\times21}$	$\tilde{d}_{2\times1\times43}, \tilde{d}_{3\times2\times14}, \tilde{d}_{1\times4\times32}$, $\tilde{d}_{1\times2\times34}, \tilde{d}_{2\times3\times41}$, $\tilde{d}_{3\times4\times12}, \tilde{d}_{4\times1\times23}$	$\tilde{c}_{3\times4}$ (6.9)	$\tilde{c}_{4\times1}, \tilde{c}_{2\times3}, \tilde{c}_{1\times2}$
		$\tilde{c}_{2\times34}$ (6.10)	$\tilde{c}_{3\times41}, \tilde{c}_{4\times12}, \tilde{c}_{1\times23}$
			$\tilde{c}_{1\times43}, \tilde{c}_{2\times14}, \tilde{c}_{3\times21}, \tilde{c}_{4\times32}$
$\tilde{d}_{1\times23\times4}$	$\tilde{d}_{2\times34\times1}, \tilde{d}_{3\times41\times2}, \tilde{d}_{4\times12\times3}$	$\tilde{c}_{12\times34}$	$\tilde{c}_{23\times41}$
$\tilde{d}_{1\times2\times3}$	$\tilde{d}_{2\times3\times4}, \tilde{d}_{3\times4\times1}, \tilde{d}_{4\times1\times2}$	$\tilde{c}_{1\times234}$	$\tilde{c}_{2\times341}, \tilde{c}_{3\times412}, \tilde{c}_{4\times123}$
		$\tilde{b}_{34}$ (6.17)	$\tilde{b}_{12}, \tilde{b}_{23}, \tilde{b}_{41}$
		$\tilde{b}_{234}$ (6.18)	$\tilde{b}_{341}, \tilde{b}_{412}, \tilde{b}_{123}$
		$\tilde{b}_{1234}$(6.19)	

A.3.1. $\tilde{d}_{4\times3\times21}$.

$$\begin{aligned}\tilde{d}_{4\times3\times21}(1^+,2^-,3^+,4^-) = \tilde{e}_{\{1^+\times2^-\times3^+\times4^-\}}\, C^{(2)}_{1\times2\times3\times4} \\ - \frac{2\,\langle2|(1+3)|4]}{\langle1|(2+3)|4]\,\langle3|(1+2)|4]}\left[\frac{\langle2\,3\rangle\,\langle2|(1+3)|4]\,s_{34}s_{123}^2}{\langle1\,2\rangle\,\langle3|(1+2)|4]^2}\right. \\ + m^2\left(2\frac{[1\,3]\,\langle4|(2+3)|1]}{[1\,2]} + \frac{[2\,3]\,\langle2|(1+3)|4]\,\langle4|(2+3)|1]}{[1\,2]\,\langle1|(2+3)|4]}\right. \\ \left.\left. + 3\frac{\langle2\,3\rangle\,\langle2|(1+3)|4]\,\langle4|(1+2)|3]}{\langle1\,2\rangle\,\langle3|(1+2)|4]}\right)\right].\end{aligned} \tag{A.28}$$

A.3.2. $\tilde{d}_{1\times23\times4}$.

$$\begin{aligned}\tilde{d}_{1\times23\times4}(1^+,2^-,3^+,4^-) = \tilde{e}_{\{1^+\times2^-\times3^+\times4^-\}}\, C^{(3)}_{1\times2\times3\times4} \\ - 2\,m^2\frac{\langle4|(2+3)|1]}{\langle1|(2+3)|4]}\left[\frac{\langle1\,2\rangle\,\langle2\,4\rangle^2}{\langle1\,4\rangle\,\langle2\,3\rangle\,\langle3\,4\rangle} + \frac{[1\,3]^2\,[3\,4]}{[1\,2]\,[1\,4]\,[2\,3]}\right].\end{aligned} \tag{A.29}$$

A.3.3. $\tilde{d}_{1\times2\times3}$.

$$\begin{aligned}\tilde{d}_{1\times2\times3}(1^+,2^-,3^+,4^-) = C^{(5)}_{1\times2\times3\times4}\,\tilde{e}_{\{1^+\times2^-\times3^+\times4^-\}} + C^{(1)}_{4\times1\times2\times3}\,\tilde{e}_{\{4^-\times1^+\times2^-\times3^+\}} \\ + \frac{\langle1\,2\rangle\,\langle2\,3\rangle}{\langle1|(2+3)|4]\,\langle3|(1+2)|4]}\left[-2\frac{s_{12}s_{23}s_{123}}{\langle1\,3\rangle^2} + 2m^2\left(2\frac{[1\,3]\,s_{123}}{\langle1\,3\rangle}\right.\right. \\ - [1\,3]^2 + \frac{[1\,2]\,[2\,3]\,\langle2\,4\rangle^2}{\langle1\,4\rangle\,\langle3\,4\rangle} - \frac{[2\,3]\,\langle2|(1+3)|4]\,\langle4|(2+3)|1]}{\langle3\,4\rangle\,\langle1|(2+3)|4]} \\ \left.\left. + \frac{[1\,2]\,\langle2|(1+3)|4]\,\langle4|(1+2)|3]}{\langle1\,4\rangle\,\langle3|(1+2)|4]}\right)\right].\end{aligned} \tag{A.30}$$

Table 4. Minimal set of integral coefficients for $A_4^{1234}(g^+, g^+, g^-, g^-; h)$. The equation numbers in brackets give the places in reference [13] where the coefficients are reported. These coefficients are the same in the scalar-mediated and fermion-mediated theories.

Coefficient	Related coefficients	Coefficient	Related coefficients
$\tilde{d}_{1\times2\times34}$	$\tilde{d}_{2\times1\times43}, \tilde{d}_{3\times4\times12}, \tilde{d}_{4\times3\times21}$	$\tilde{c}_{2\times3}$ (7.10)	$\tilde{c}_{4\times1}$
$\tilde{d}_{1\times4\times32}$	$\tilde{d}_{3\times2\times14}, \tilde{d}_{4\times1\times23}, \tilde{d}_{2\times3\times41}$	$\tilde{c}_{1\times23}$ (7.11)	$\tilde{c}_{2\times14}, \tilde{c}_{3\times41}, \tilde{c}_{4\times32}$
$\tilde{d}_{2\times34\times1}$	$\tilde{d}_{4\times12\times3}$	$\tilde{c}_{1\times234}$	$\tilde{c}_{2\times341}, \tilde{c}_{3\times412}, \tilde{c}_{4\times123}$
$\tilde{d}_{1\times23\times4}$	$\tilde{d}_{3\times41\times2}$	$\tilde{c}_{23\times41}$	
$\tilde{d}_{1\times2\times3}$	$\tilde{d}_{3\times4\times1}, \tilde{d}_{4\times1\times2}, \tilde{d}_{2\times3\times4}$	$\tilde{b}_{23}$ (7.17)	$\tilde{b}_{41}$
		$\tilde{b}_{234}$ (7.18)	$\tilde{b}_{341}, \tilde{b}_{412}, \tilde{b}_{123}$
		$\tilde{b}_{1234}$ (7.19)	

A.3.4. $\tilde{c}^{(0)}_{12\times34}$, $\tilde{c}^{(2)}_{12\times34}$. In this case the scalar coefficient $\tilde{c}^{(0)}_{12\times34}(1^+, 2^-, 3^+, 4^-)$ has been given previously, in equation (6.13) of reference [13]. Moreover, $\tilde{c}^{(2)}_{12\times34}(1^+, 2^-, 3^+, 4^-) = c^{(2)}_{12\times34}(1^+, 2^-, 3^+, 4^-)$, where the fermionic coefficient is given in equation (6.12) of reference [13].

A.3.5. $\tilde{c}^{(0)}_{1\times234}$, $\tilde{c}^{(2)}_{1\times234}$.

$$\tilde{c}^{(0)}_{1\times234}(1^+, 2^-, 3^+, 4^-) = -2(s_{12} + s_{13} + s_{14}) \frac{s_{234} \langle 1|(2+4)|3]^2}{[2\,3]\ [3\,4]\ \langle 1|(2+3)|4]^3 \langle 1|(3+4)|2]^3} \times \left([2\,3]^2 \langle 1|(2+3)|4]^2 + [3\,4]^2 \langle 1|(3+4)|2]^2 \right). \tag{A.31}$$

In addition, we have $\tilde{c}^{(2)}_{1\times234}(1^+, 2^-, 3^+, 4^-) = c^{(2)}_{1\times234}(1^+, 2^-, 3^+, 4^-)$, where the fermionic coefficient is given in equation (6.16) of reference [13].

A.4. Coefficients for $A_4^{1234}(g^+, g^+, g^-, g^-; h)$

The effective pentagon coefficients are given by

$$\tilde{e}_{\{1^+\times2^+\times3^-\times4^-\}} = -4\,m^4 \frac{[1\,2]\,\langle 3\,4\rangle}{\langle 1\,2\rangle\,[3\,4]}, \tag{A.32}$$

$$\tilde{e}_{\{2^+\times3^-\times4^-\times1^+\}} = -4\,m^4 \frac{[2\,3]\ \langle 3\,4\rangle^2\ [4\,1]}{\langle 2\,3\rangle\ [3\,4]^2\ \langle 4\,1\rangle}, \tag{A.33}$$

$$\tilde{e}_{\{2^+\times3^-\times4^-\times1^+\}} = -4\,m^4 \frac{[2\,3]\ \langle 3\,4\rangle^2\ [4\,1]}{\langle 2\,3\rangle\ [3\,4]^2\ \langle 4\,1\rangle}, \tag{A.34}$$

$$\tilde{e}_{\{4^-\times1^+\times2^+\times3^-\}} = \tilde{e}_{\{2^+\times3^-\times4^-\times1^+\}}\{2 \leftrightarrow 4, 1 \leftrightarrow 3, \langle\,\rangle \leftrightarrow [\,]\}. \tag{A.35}$$

The minimal set of coefficients that needs to be calculated is given in table 4.

A.4.1. $\tilde{d}_{1\times2\times34}$.

$$\tilde{d}_{1\times2\times34}(1^+, 2^+, 3^-, 4^-) = \mathcal{C}^{(4)}_{1\times2\times3\times4}\, \tilde{e}_{\{1^+\times2^+\times3^-\times4^-\}}. \tag{A.36}$$

A.4.2. $\tilde{d}_{1\times4\times32}$.

$$\begin{aligned}\tilde{d}_{1\times4\times32}(1^+,2^+,3^-,4^-) = {} & \mathcal{C}^{(2)}_{2\times3\times4\times1}\,\tilde{e}_{\{2^+\times3^-\times4^-\times1^+\}} \\ & - 2\,\frac{[2\,4]^2}{\langle1|(2+3)|4]\;[3\,4]}\left\{\frac{s_{14}\,s_{234}^2\,\langle1|(3+4)|2]}{[2\,3]\;\langle1|(2+3)|4]^2}\right. \\ & + m^2\left[3\,\frac{\langle1|(3+4)|2]\,\langle4|(2+3)|1]}{[2\,3]\,\langle1|(2+3)|4]}\right. \\ & \left.\left. + \frac{[1\,4]\,\langle3\,4\rangle\,s_{234}}{\langle2\,3\rangle\,[2\,4]\,[3\,4]} + \frac{\langle3\,4\rangle\;\langle3|(2+4)|1]}{\langle2\,3\rangle\,[2\,4]}\right]\right\}.\end{aligned} \tag{A.37}$$

A.4.3. $\tilde{d}_{2\times34\times1}$.

$$\begin{aligned}\tilde{d}_{2\times34\times1}(1^+,2^+,3^-,4^-) = {} & \mathcal{C}^{(3)}_{2\times3\times4\times1}\,\tilde{e}_{\{2^+\times3^-\times4^-\times1^+\}} \\ & - 2\,m^2\frac{\langle3\,4\rangle\;\langle1|(3+4)|2]\;\langle2|(3+4)|1]}{\langle1\,2\rangle\;\langle1\,4\rangle\;\langle2\,3\rangle\;[3\,4]^2}.\end{aligned} \tag{A.38}$$

A.4.4. $\tilde{d}_{1\times23\times4}$.

$$\begin{aligned}\tilde{d}_{1\times23\times4}(1^+,2^+,3^-,4^-) = {} & \mathcal{C}^{(3)}_{1\times2\times3\times4}\,\tilde{e}_{\{1^+\times2^+\times3^-\times4^-\}} + 2\,m^2\,\frac{\langle4|(2+3)|1]}{\langle1\,2\rangle\;[3\,4]\;\langle1|(2+3)|4]} \\ & \times\left[\frac{s_{12}[2\,4]^2}{[1\,4]\;[2\,3]} + \frac{s_{34}\langle1\,3\rangle^2}{\langle2\,3\rangle\;\langle1\,4\rangle}\right].\end{aligned} \tag{A.39}$$

A.4.5. $\tilde{d}_{1\times2\times3}$.

$$\begin{aligned}\tilde{d}_{1\times2\times3}(1^+,2^+,3^-,4^-) = {} & \mathcal{C}^{(5)}_{1\times2\times3\times4}\,\tilde{e}_{\{1^+\times2^+\times3^-\times4^-\}} + \mathcal{C}^{(1)}_{4\times1\times2\times3}\,\tilde{e}_{\{4^-\times1^+\times2^+\times3^-\}} \\ & - 2\,m^2\frac{[1\,2]^2\;\langle2\,3\rangle}{\langle1\,2\rangle\;[1\,4]\;[3\,4]}.\end{aligned} \tag{A.40}$$

A.4.6. $\tilde{c}^{(0)}_{23\times41}, \tilde{c}^{(2)}_{23\times41}$.

$$\begin{aligned}\tilde{c}^{(0)}_{23\times41}(1^+,2^+,3^-,4^-) = {} & -\tilde{c}^{(0)}_{12\times34}(2^+,3^-,1^+,4^-) \\ & - \left\{2\,\Delta_3(1,4,2,3)\left[\frac{(s_{13}-s_{24})}{\langle2|(1+4)|3]\;\langle1|(2+3)|4]}\right]^2\right. \\ & \left. + 4\,\frac{\langle3|(1+4)|2]\;\langle4|(2+3)|1]}{\langle2|(1+4)|3]\;\langle1|(2+3)|4]}\right\}.\end{aligned} \tag{A.41}$$

Table 5. Minimal set of integral coefficients for $A_4^{34}(1_{\bar{q}}^+, 2_q^-, 3_g^+, 4_g^+)$, $A_4^{34}(1_{\bar{q}}^+, 2_q^-, 3_g^-, 4_g^+)$ and $A_4^{34}(1_{\bar{q}}^+, 2_q^-, 3_g^+, 4_g^-)$ together with the related coefficients that can be obtained from the base set. The equation numbers in brackets give the places in reference [13] where the coefficients are reported. These coefficients are the same in the scalar-mediated and fermion-mediated theories.

$1_{\bar{q}}^+, 2_q^-, 3_g^+, 4_g^+$		$1_{\bar{q}}^+, 2_q^-, 3_g^-, 4_g^+$		$1_{\bar{q}}^+, 2_q^-, 3_g^+, 4_g^-$
Coefficient	Related coefficient	Coefficient	Related coefficient	Coefficient
$\tilde{d}_{3\times21\times4}$	$\tilde{d}_{3\times4\times12}$	$\tilde{d}_{3\times21\times4}$	$\tilde{d}_{3\times4\times12}$	$\tilde{c}_{4\times123}$
$\tilde{d}_{4\times3\times21}$		$\tilde{d}_{4\times3\times21}$		$\tilde{b}_{123}$ (10.4)
$\tilde{c}_{3\times21}$ (8.4)	$\tilde{c}_{4\times12}$	$\tilde{c}_{3\times4}$ (9.3)		
$\tilde{c}_{12\times34}$		$\tilde{c}_{3\times21}$ (9.4)	$\tilde{c}_{4\times12}$	
$\tilde{c}_{4\times123}$		$\tilde{c}_{12\times34}$		
$\tilde{c}_{3\times412}$		$\tilde{c}_{4\times123}$	$\tilde{c}_{3\times412}$	
$\tilde{b}_{12}$ (8.11)		$\tilde{b}_{34}$ (9.9)		
$\tilde{b}_{123}$ (8.12)		$\tilde{b}_{12}$ (9.10)		
$\tilde{b}_{412}$ (8.13)		$\tilde{b}_{123}$ (9.11)	$\tilde{b}_{412}$	
$\tilde{b}_{1234}$ (8.14)		$\tilde{b}_{1234}$ (9.12)		

Moreover, $\tilde{c}^{(2)}_{23\times41}(1^+,2^+,3^-,4^-) = c^{(2)}_{23\times41}(1^+,2^+,3^-,4^-)$, where the fermionic coefficient is given in equation (7.14) of reference [13].

A.4.7. $\tilde{c}^{(0)}_{1\times234}, \tilde{c}^{(2)}_{1\times234}$.

$$\tilde{c}^{(0)}_{1\times234}(1^+,2^+,3^-,4^-) = -2\,(s_{12}+s_{13}+s_{14})\,s_{234}\,\frac{\langle1|(3+4)|2]\,[2\,4]^2}{\langle1|(2+3)|4]^3\,[2\,3]\,[3\,4]}. \tag{A.42}$$

Furthermore, $\tilde{c}^{(2)}_{1\times234}(1^+,2^+,3^-,4^-) = c^{(2)}_{1\times234}(1^+,2^+,3^-,4^-)$, where the fermionic coefficient is given in equation (7.16) of reference [13].

A.5. Coefficients for $A_4^{34}(\bar{q}^+, q^-, g^+, g^+; h)$

The coefficients that must be computed for this amplitude are shown in the left-hand column of table 5.

A.5.1. $\tilde{d}_{3\times21\times4}$.

$$\begin{aligned}\tilde{d}_{3\times21\times4}(1_{\bar{q}}^+,2_q^-,3_g^+,4_g^+) = -2\,\frac{\langle2\,4\rangle\,\langle2\,3\rangle}{\langle1\,2\rangle\,\langle3\,4\rangle^3}\,[(s_{13}+s_{23})\,(s_{14}+s_{24})-s_{12}\,s_{34}]\\ +2\,m^2\left[\frac{[1\,3]\,[1\,4]}{[1\,2]\,\langle3\,4\rangle}+3\,\frac{\langle2\,3\rangle\,\langle2\,4\rangle\,[3\,4]}{\langle1\,2\rangle\,\langle3\,4\rangle^2}\right].\end{aligned} \tag{A.43}$$

A.5.2. $\tilde{d}_{4\times3\times21}$.

$$\tilde{d}_{4\times3\times21}(1_{\bar{q}}^+,2_q^-,3_g^+,4_g^+) = 2\,m^2\,\frac{[3\,4]}{\langle3\,4\rangle}\left[\frac{\langle2\,3\rangle\,\langle2|(1+3)|4]}{\langle1\,2\rangle\,\langle3|(1+2)|4]}-\frac{[1\,3]\,\langle4|(2+3)|1]}{[1\,2]\,\langle4|(1+2)|3]}\right]. \tag{A.44}$$

A.5.3. $\tilde{c}^{(0)}_{12\times34}, \tilde{c}^{(2)}_{12\times34}$.

$$\tilde{c}^{(0)}_{12\times34}(1^+_{\bar{q}}, 2^-_q, 3^+_g, 4^+_g) = 0. \tag{A.45}$$

The coefficient $\tilde{c}^{(2)}_{12\times34}(1^+_{\bar{q}}, 2^-_q, 3^+_g, 4^+_g)$ is identical to $c^{(2)}_{12\times34}(1^+_{\bar{q}}, 2^-_q, 3^+_g, 4^+_g)$ given in equation (8.6) of reference [13].

A.5.4. $\tilde{c}^{(0)}_{4\times123}, \tilde{c}^{(2)}_{4\times123}$.

$$\tilde{c}^{(0)}_{4\times123}(1^+_{\bar{q}}, 2^-_q, 3^+_g, 4^+_g) = -2\,(s_{14} + s_{24} + s_{34})\left[\frac{\langle 2\,3\rangle\ \langle 2\,4\rangle}{\langle 1\,2\rangle\ \langle 3\,4\rangle^3}\right]. \tag{A.46}$$

The coefficient $\tilde{c}^{(2)}_{4\times123}(1^+_{\bar{q}}, 2^-_q, 3^+_g, 4^+_g)$ is identical to $c^{(2)}_{4\times123}(1^+_{\bar{q}}, 2^-_q, 3^+_g, 4^+_g)$ given in equation (8.8) of reference [13].

A.5.5. $\tilde{c}^{(0)}_{3\times412}, \tilde{c}^{(2)}_{3\times412}$.

$$\tilde{c}^{(0)}_{3\times412}(1^+_{\bar{q}}, 2^-_q, 3^+_g, 4^+_g) = -2\,(s_{13} + s_{23} + s_{34})\left[\frac{\langle 2\,3\rangle\ \langle 2\,4\rangle}{\langle 1\,2\rangle\ \langle 3\,4\rangle^3}\right]. \tag{A.47}$$

The coefficient $\tilde{c}^{(2)}_{3\times412}(1^+_{\bar{q}}, 2^-_q, 3^+_g, 4^+_g)$ is identical to $c^{(2)}_{3\times412}(1^+_{\bar{q}}, 2^-_q, 3^+_g, 4^+_g)$ given in equation (8.10) of reference [13].

A.6. Coefficients for $A^{34}_4(\bar{q}^+, q^-, g^-, g^+; h)$

The coefficients that must be computed for this amplitude are shown in the middle column of table 5.

A.6.1. $\tilde{d}_{3\times21\times4}$.

$$\tilde{d}_{3\times21\times4}(1^+_{\bar{q}}, 2^-_q, 3^-_g, 4^+_g) = 2\,m^2\,\frac{\langle 3|(1+2)|4]}{\langle 4|(1+2)|3]}\left[\frac{\langle 2\,3\rangle\ \langle 2\,4\rangle}{\langle 1\,2\rangle\ \langle 3\,4\rangle} - \frac{[1\,3]\ [1\,4]}{[1\,2]\ [3\,4]}\right]. \tag{A.48}$$

A.6.2. $\tilde{d}_{4\times3\times21}$.

$$\begin{aligned}\tilde{d}_{4\times3\times21}(1^+_{\bar{q}}, 2^-_q, 3^-_g, 4^+_g) = \frac{-2}{\langle 4|(1+2)|3]}\Bigg\{&\frac{[1\,3]\ \langle 4|(2+3)|1]\ s_{34}\,s^2_{123}}{[1\,2]\ \langle 4|(1+2)|3]^2}\\ &+ m^2\left[\frac{3\ [1\,3]\ \langle 3|(1+2)|4]\ \langle 4|(2+3)|1]}{[1\,2]\ \langle 4|(1+2)|3]}\right.\\ &\left.+\ \frac{\langle 2\,3\rangle\ \langle 2|(1+3)|4]}{\langle 1\,2\rangle}\right]\Bigg\}.\end{aligned} \tag{A.49}$$

A.6.3. $\tilde{c}^{(0)}_{12\times34}, \tilde{c}^{(2)}_{12\times34}$.

$$
\begin{aligned}
&\tilde{c}^{(0)}_{12\times34}(1^+_{\bar{q}}, 2^-_q, 3^-_g, 4^+_g) \\
&\quad = 8\,(s_{124} - s_{123})\,(s_{12} + s_{34} + 2\,s_{13} + 2\,s_{23})\,\frac{\langle 2\,4\rangle\ [1\,3]\ \langle 3|(1+2)|4]}{\langle 4|(1+2)|3]^2 \Delta_3(1,2,3,4)} \\
&\qquad + \big((9\,s_{13} - 7\,s_{23} - s_{14} - s_{24} + 4\,s_{34})\ \langle 2\,4\rangle\ [1\,4] \\
&\qquad - (9\,s_{14} - 7\,s_{24} - s_{13} - s_{23} + 4\,s_{34})\ \langle 2\,3\rangle\ [1\,3]\big) \times \frac{1}{\langle 4|(1+2)|3]^2} \\
&\qquad + 12\,\frac{s_{1234}\,((s_{13}+s_{23})^2 - (s_{14}+s_{24})^2)\ \langle 2|(3+4)|1]\ \langle 3|(1+2)|4]}{\langle 4|(1+2)|3]\ \Delta_3(1,2,3,4)^2} \\
&\qquad + 4\ \big(\{3\,(s_{12}+s_{34}) + 4\,(s_{13}+s_{23}+s_{14})\}\ [1\,3]\ \langle 2\,3\rangle \\
&\qquad - \{3\,(s_{12}+s_{34}) + 4\,(s_{13}+s_{24}+s_{14})\}\ [1\,4]\ \langle 2\,4\rangle\big) \times \frac{\langle 3|(1+2)|4]}{\langle 4|(1+2)|3]\ \Delta_3(1,2,3,4)} \\
&\qquad - 24\,\frac{[1\,3]\ \langle 2\,4\rangle\ \langle 3|(1+2)|4]^2}{\langle 4|(1+2)|3]\ \Delta_3(1,2,3,4)} - 8\,\frac{[1\,4]\ \langle 2\,3\rangle\ \langle 3|(1+2)|4]}{\Delta_3(1,2,3,4)} + 8\,\frac{[1\,4]\ \langle 2\,3\rangle}{\langle 4|(1+2)|3]} \\
&\qquad + \Bigg\{\frac{2\,\langle 2\,4\rangle^2\ [3\,4]\ (s_{14}+s_{24})^2}{\langle 1\,2\rangle\ \langle 4|(1+2)|3]^3} + \frac{[1\,3]\ \langle 2\,4\rangle\ (s_{14}+s_{24})\,(4\,s_{124} - 2\,s_{34})}{\langle 4|(1+2)|3]^3} \\
&\qquad + \frac{2\ \langle 2\,3\rangle\ \langle 2\,4\rangle\ [3\,4]\ (s_{14}+s_{24})}{\langle 1\,2\rangle\ \langle 4|(1+2)|3]^2} - \frac{\langle 2\,3\rangle\ [1\,3]\ (s_{14}+s_{24}-s_{13}-s_{23})}{\langle 4|(1+2)|3]^2}\Bigg\} \\
&\qquad - \{1 \leftrightarrow 2, 3 \leftrightarrow 4, \langle\,\rangle \leftrightarrow [\,]\}\,.
\end{aligned}
\tag{A.50}
$$

The coefficient $\tilde{c}^{(2)}_{12\times34}(1^+_{\bar{q}}, 2^-_q, 3^-_g, 4^+_g)$ is identical to $c^{(2)}_{12\times34}(1^+_{\bar{q}}, 2^-_q, 3^-_g, 4^+_g)$ given in equation (9.6) of reference [13].

A.6.4. $\tilde{c}^{(0)}_{4\times123}, \tilde{c}^{(2)}_{4\times123}$.

$$
\tilde{c}^{(0)}_{4\times123}(1^+_{\bar{q}}, 2^-_q, 3^-_g, 4^+_g) = -\frac{2\,(s_{14}+s_{24}+s_{34})\ [1\,3]\ \langle 4|(2+3)|1]\ s_{123}}{[1\,2]\ \langle 4|(1+2)|3]^3}. \tag{A.51}
$$

The coefficient $\tilde{c}^{(2)}_{4\times123}(1^+_{\bar{q}}, 2^-_q, 3^-_g, 4^+_g)$ is identical to $c^{(2)}_{4\times123}(1^+_{\bar{q}}, 2^-_q, 3^-_g, 4^+_g)$ given in equation (9.8) of reference [13].

A.7. Coefficients for $A^{34}_4(\bar{q}^+, q^-, g^+, g^-; h)$

The coefficients for this amplitude that cannot be obtained from those for $H^{34}_4(\bar{q}^+, q^-, g^-, g^+)$ by performing the following operation: $1 \leftrightarrow 2, \langle\rangle \leftrightarrow []$ are listed in the right-most column of table 5. The explicit form of $\tilde{c}_{4\times123}$ is given here, whereas b_{123} remains unaltered as compared to the fermion case.

A.7.1. $\tilde{c}^{(0)}_{4\times123}, \tilde{c}^{(2)}_{4\times123}$.

$$\tilde{c}^{(0)}_{4\times123}(1^+_{\bar{q}}, 2^-_q, 3^+_g, 4^-_g) = \frac{2\,\langle 2|(1+3)|4]\; s_{123}}{\langle 1\,2\rangle\;\langle 3|(1+2)|4]^2}\left\{\langle 2\,4\rangle - \langle 3\,4\rangle\,\frac{\langle 2|(1+3)|4]}{\langle 3|(1+2)|4]}\right\}. \tag{A.52}$$

The coefficient $\tilde{c}^{(2)}_{4\times123}(1^+_{\bar{q}}, 2^-_q, 3^+_g, 4^-_g)$ is identical to $c^{(2)}_{4\times123}(1^+_{\bar{q}}, 2^-_q, 3^+_g, 4^-_g)$ given in equation (10.3) of reference [13].

A.8. Amplitude for $0 \to \bar{q}q\bar{q}qh$

This calculation proceeds in a similar way to the calculation for a loop of fermions detailed in reference [34]. The amplitude can be obtained by considering the tensor current for the scalar-mediated process $0 \to ggh$, with two off-shell gluons (with momenta k_1 and k_2),

$$\mathcal{T}^{\mu_1\mu_2}(k_1,k_2) = -i\delta^{c_1c_2}\,\frac{g_s^2}{8\pi^2}\left(\frac{-\lambda}{4}\right)\left[\tilde{F}_{\rm T}(k_1,k_2)\,T_{\rm T}^{\mu_1\mu_2} + \tilde{F}_{\rm L}(k_1,k_2)\,T_{\rm L}^{\mu_1\mu_2}\right]. \tag{A.53}$$

The two tensor structures appearing here are

$$T_{\rm T}^{\mu_1\mu_2} = k_1\cdot k_2\,g^{\mu_1\mu_2} - k_1^{\mu_2}k_2^{\mu_1}, \tag{A.54}$$

$$T_{\rm L}^{\mu_1\mu_2} = k_1^2k_2^2\,g^{\mu_1\mu_2} - k_1^2\,k_2^{\mu_1}k_2^{\mu_2} - k_2^2\,k_1^{\mu_1}k_1^{\mu_2} + k_1\cdot k_2\,k_1^{\mu_1}k_2^{\mu_2}, \tag{A.55}$$

and the form factors are given by

$$\begin{aligned}\tilde{F}_{\rm T}(k_1,k_2) = -\frac{1}{\Delta(k_1,k_2)}\big\{&k_{12}^2\,(B_0(k_1;m)+B_0(k_2;m)-2B_0(k_{12};m))\\ &-2\,k_1\cdot k_{12}\,k_2\cdot k_{12}\,C_0(k_1,k_2;m)\\ &+(k_1^2-k_2^2)\,(B_0(k_1;m)-B_0(k_2;m))\big\} - k_1\cdot k_2\,\tilde{F}_{\rm L}(k_1,k_2),\end{aligned} \tag{A.56}$$

$$\begin{aligned}\tilde{F}_{\rm L}(k_1,k_2) = -\frac{1}{\Delta(k_1,k_2)}\Bigg\{&\left[2-\frac{3k_1^2\,k_2\cdot k_{12}}{\Delta(k_1,k_2)}\right](B_0(k_1;m)-B_0(k_{12};m))\\ &+\left[2-\frac{3k_2^2\,k_1\cdot k_{12}}{\Delta(k_1,k_2)}\right](B_0(k_2;m)-B_0(k_{12};m))\\ &-\left[4m^2+k_1^2+k_2^2+k_{12}^2-3\frac{k_1^2\,k_2^2\,k_{12}^2}{\Delta(k_1,k_2)}\right]C_0(k_1,k_2;m)-2\Bigg\},\end{aligned} \tag{A.57}$$

where $k_{12} = k_1 + k_2$ and $\Delta(k_1,k_2) = k_1^2\,k_2^2 - (k_1\cdot k_2)^2$. As expected, the rational and bubble coefficients are identical to the case for a fermion loop. By contracting equation (A.55) with currents for the quark–antiquark lines, we then arrive at the result for the amplitude. All helicity combinations can be obtained from permutations of the single expression

$$\begin{aligned}A_4^{4q}(1^+_q, 2^-_q, 3^+_{\bar{q}}, 4^-_{\bar{q}}; h) = &\left[\frac{\langle 2|(3+4)|1]\;\langle 4|(1+2)|3] + \langle 2\,4\rangle\;[1\,3]\;(2\,p_{12}.p_{34})}{s_{12}\,s_{34}}\right]\\ &\times\tilde{F}_{\rm T}(p_{12},p_{34}) + 2\;\langle 2\,4\rangle\;[1\,3]\;\tilde{F}_{\rm L}(p_{12},p_{34}).\end{aligned} \tag{A.58}$$

Table 6. Numerical values of coefficients of the *ggggh* process not already reported in reference [13] at kinematic point (B.1).

Helicities	Coefficient	Real Part	Imaginary Part	Absolute Value
++++	$\tilde{d}_{1\times2\times34}$	−0.984 061 3828	−0.514 432 3508	1.110 413 1883
	$\tilde{d}_{1\times23\times4}$	−3.354 895 7407	−4.843 220 6981	5.891 698 5803
	$\tilde{d}_{1\times2\times3}$	−6.744 591 0748	−15.466 394 2318	16.873 021 6411
	$\tilde{c}_{1\times234}$	−10.636 876 2164	−31.682 984 0771	33.420 870 9592
+++−	$\tilde{d}_{1\times2\times34}$	23.445 129 5603	18.599 644 1921	29.926 925 4046
	$\tilde{d}_{1\times4\times32}$	20.507 168 8388	27.445 139 3815	34.260 467 7355
	$\tilde{d}_{2\times1\times43}$	−4.900 993 6782	42.122 517 6136	42.406 676 7047
	$\tilde{d}_{2\times34\times1}$	−44.384 546 3184	−38.333 996 4812	58.647 107 6705
	$\tilde{d}_{4\times3\times21}$	−7.120 381 1993	0.688 621 6537	7.153 602 4635
	$\tilde{d}_{1\times23\times4}$	−1.800 583 5535	1.535 112 9014	2.366 151 4646
	$\tilde{d}_{2\times3\times4}$	0.820 615 5641	1.473 521 0192	1.686 616 1680
	$\tilde{d}_{1\times2\times3}$	−19.239 784 7846	−1.476 292 5832	19.296 340 5429
	$\tilde{d}_{3\times4\times1}$	−0.331 678 8675	1.611 469 2592	1.645 248 9309
	$\tilde{c}_{4\times123}$	−11.061 653 8761	−1.791 633 9105	11.205 808 2504
	$\tilde{c}_{1\times234}$	18.964 670 2722	24.451 016 7733	30.943 673 6633
	$\tilde{c}_{2\times341}$	−8.993 451 4290	11.193 435 5822	14.358 801 0899
	$\tilde{c}_{12\times34}$	−3.746 138 9306	21.049 348 3972	21.380 098 8032
+−+−	$\tilde{d}_{4\times3\times21}$	−6.936 823 5764	−13.422 076 9362	15.108 662 1053
	$\tilde{d}_{1\times23\times4}$	−5.400 516 1311	3.828 193 9917	6.619 716 2870
	$\tilde{d}_{1\times2\times3}$	−21.099 780 3781	−62.360 830 8275	65.833 684 0341
	$\tilde{c}_{12\times34}$	−39.740 334 0718	22.210 411 3517	45.525 778 6814
	$\tilde{c}_{1\times234}$	3.968 212 5956	13.481 379 1531	14.053 266 3489
++−−	$\tilde{d}_{1\times2\times34}$	−0.026 753 0609	−1.110 090 8623	1.110 413 1883
	$\tilde{d}_{1\times4\times32}$	22.651 897 0482	−458.124 839 8611	458.684 507 4097
	$\tilde{d}_{2\times34\times1}$	64.231 654 8189	−59.023 356 2841	87.232 230 6708
	$\tilde{d}_{1\times23\times4}$	−5.745 078 5528	3.288 573 5727	6.619 716 2870
	$\tilde{d}_{1\times2\times3}$	−10.895 434 6530	−12.883 647 1165	16.873 021 6411
	$\tilde{c}_{23\times41}$	1075.318 606 8541	747.629 089 1424	1309.679 106 1854
	$\tilde{c}_{1\times234}$	36.885 622 0760	−309.117 237 7677	311.310 160 1314

Appendix B. Numerical value of coefficients at a given phase-space point

Tables 6 and 7 contain numerical results for the integral coefficients for the *ggggh* and $\bar{q}qggh$ amplitudes, respectively, at the phase-space point ($p = (E, p_x, p_y, p_z)$):

$$\begin{aligned} p_1 &= (-15\kappa, -10\kappa, +11\kappa, +2\kappa), \\ p_2 &= (-9\kappa, +8\kappa, +1\kappa, -4\kappa), \\ p_3 &= (-21\kappa, +4\kappa, -13\kappa, +16\kappa), \\ p_4 &= (-7\kappa, +2\kappa, -6\kappa, +3\kappa), \\ p_h &= (+52\kappa, -4\kappa, +7\kappa, -17\kappa), \end{aligned} \tag{B.1}$$

with $\kappa = 1/\sqrt{94}$ and $p_h = -p_1 - p_2 - p_3 - p_4$. This fixes $s_{1234} = 25$, $m_h = 5$ and we further choose $m = 1.5$.

Table 7. Numerical values of coefficients of the $\bar{q}qggh$ process that differ from reference [13] at kinematic point (B.1).

Helicities	Coefficient	Real Part	Imaginary Part	Absolute Value
$+-++$	$d_{3\times21\times4}$	370.433 539 2027	1300.470 465 9852	1352.199 852 0434
	$d_{4\times3\times21}$	0.922 007 9194	−4.007 760 9078	4.112 450 1332
	$c_{12\times34}$	−13.767 289 9406	−4.387 153 9915	14.449 408 0313
	$c_{4\times123}$	25.101 460 9317	92.881 358 4055	96.213 461 0133
	$c_{3\times412}$	67.153 204 4289	252.146 232 6711	260.935 385 7094
$+--+$	$d_{3\times21\times4}$	20.896 007 3185	19.965 647 8672	28.901 041 7911
	$d_{4\times3\times21}$	−0.426 797 1904	−3.814 930 2668	3.838 730 1002
	$c_{12\times34}$	−9.098 735 3955	−7.631 435 1405	11.875 427 9123
	$c_{4\times123}$	1.945 068 6855	1.931 499 4054	2.741 164 3775
$+-+-$	$c_{4\times123}$	5.205 078 5566	1.186 433 7667	5.338 582 9453

Due to the correspondence of results between the scalar and fermionic loop cases, many of these values have already been reported in reference [13]. Tables 6 and 7 therefore contain only the coefficients that differ from the fermionic case.

After including the integrals and rational terms, the values of the colour-ordered subamplitudes are

$$\begin{aligned}
A^{1234}(1^+,2^+,3^+,4^+;h) &= -26.505\,233\,03 - 3.722\,078\,577\,i,\\
|A^{1234}(1^+,2^+,3^+,4^+;h)| &= 26.765\,299\,30,\\
A^{1234}(1^+,2^+,3^+,4^-;h) &= 10.005\,500\,42 + 10.391\,302\,52\,i,\\
|A^{1234}(1^+,2^+,3^+,4^-;h)| &= 14.425\,297\,46,\\
A^{1234}(1^+,2^-,3^+,4^-;h) &= 2.105\,330\,472 - 3.500\,785\,469\,i,\\
|A^{1234}(1^+,2^-,3^+,4^-;h)| &= 4.085\,084\,491,\\
A^{1234}(1^+,2^+,3^-,4^-;h) &= -0.788\,758\,613 + 0.151525\,137\,i,\\
|A^{1234}(1^+,2^+,3^-,4^-;h)| &= 0.803\,181\,185.
\end{aligned} \tag{B.2}$$

$$\begin{aligned}
A^{34}(1^+,2^-,3^+,4^+;h) &= -3.151\,452\,974 + 5.766\,222\,683\,i,\\
|A^{34}(1^+,2^-,3^+,4^+;h)| &= 6.571\,223\,621,\\
A^{34}(1^+,2^-,3^-,4^+;h) &= 1.375\,544\,184 + 1.088\,612\,645\,i,\\
|A^{34}(1^+,2^-,3^-,4^+;h)| &= 1.754\,194\,771,\\
A^{34}(1^+,2^-,3^+,4^-;h) &= 3.032\,201\,250 - 1.275\,260\,855\,i,\\
|A^{34}(1^+,2^-,3^+,4^-;h)| &= 3.289\,458\,111.
\end{aligned} \tag{B.3}$$

$$\begin{aligned}
A^{4q}(1^+,2^-,3^+,4^-;h) &= 1.583\,011\,630 - 1.072\,246\,795\,i,\\
|A^{4q}(1^+,2^-,3^+,4^-;h)| &= 1.911\,972\,544.
\end{aligned} \tag{B.4}$$

Appendix C. Large mass limit

Using equation (2.2) and the large mass expansion for the scalar triangle integral,

$$C_0(p_1, p_2; m) \to -\frac{1}{2\,m^2} - \frac{s}{24m^4} + O\left(\frac{1}{m^6}\right), \quad s = m_h^2 = 2p_1 \cdot p_2, \tag{C.1}$$

we can extract the effective interaction for the fermionic theory:

$$\mathcal{L}_{hgg} = -\frac{1}{4} C_{\rm f} G_a^{\mu\nu}\, G_{\mu\nu\, a}\, h, \quad C_{\rm f} = -\frac{g_{\rm s}^2}{12\pi^2\, v}, \tag{C.2}$$

valid when $m_h^2 \ll m^2$. From equation (2.3) the corresponding effective Lagrangian for the scalar loop is

$$\mathcal{L}_{hgg} = -\frac{1}{4} C_{\rm s} G_a^{\mu\nu}\, G_{\mu\nu\, a}\, h, \quad C_{\rm s} = \frac{g_{\rm s}^2}{24\pi^2 m^2}\left(-\frac{\lambda}{4}\right). \tag{C.3}$$

From these equations we see that

$$\frac{\left(\frac{m^2}{v}\right) C_{\rm s}}{\left(\frac{-\lambda}{4}\right) C_{\rm f}} = -\frac{1}{2}. \tag{C.4}$$

So, in our canonical normalization in which the coupling factors shown on the left-hand side of equation (C.4) are extracted, the amplitudes for the fermion- and scalar-mediated cases are related in the large-mass (EFT) limit by a factor of $-1/2$. In other words,

$$m^2 A(\ldots; h) \to -\frac{1}{2} m^2 H(\ldots; h), \tag{C.5}$$

where the asymptotic forms for the fermion-mediated amplitudes $m^2 H(\ldots; h)$ are given in appendix B of reference [13].

ORCID iDs

R Keith Ellis https://orcid.org/0000-0002-5854-1788

References

[1] Anastasiou C *et al* 2016 High precision determination of the gluon fusion Higgs boson cross-section at the LHC *J. High Energy Phys.* JHEP05(2016)058
[2] Mistlberger B 2018 Higgs boson production at hadron colliders at N^{3}LO in QCD *J. High Energy Phys.* JHEP05(2018)028
[3] CMS Collaboration 2019 Measurement of inclusive and differential Higgs boson production cross sections in the diphoton decay channel in proton–proton collisions at $s = 13$ TeV *J. High Energy Phys.* JHEP01(2019)183
[4] ATLAS Collaboration Measurement of the properties of Higgs boson production at $\sqrt{s}$=13 TeV in the $H\to\gamma\gamma$ channel using 139 fb^{-1} of pp collision data with the ATLAS experiment 28 July –6 August 2020 Prague, Czech Republic *40th Int. Conf. on High Energy Physics (ICHEP), ATLAS-CONF-2020-026* ATLAS Collaboration Measurement of the properties of Higgs boson production at s = 13 TeV in the $H \to \gamma\gamma$ channel using 139 fb^{-1} of pp collision data with the ATLAS experiment.
[5] Bonciani R, Degrassi G and Vicini A 2007 Scalar particle contribution to Higgs production via gluon fusion at NLO *J. High Energy Phys.* JHEP112007095

[6] Brein O and Hollik W 2007 Distributions for MSSM Higgs boson + jet production at hadron colliders *Phys. Rev.* D **76** 035002
[7] Grojean C, Salvioni E, Schlaffer M and Weiler A 2014 Very boosted Higgs in gluon fusion *J. High Energy Phys.* JHEP05(2014)002
[8] Banfi A, Bond A, Martin A and Sanz V 2018 Digging for top squarks from Higgs data: from signal strengths to differential distributions *J. High Energy Phys.* JHEP11(2018)171
[9] Espinosa J R, Grojean C, Sanz V and Trott M 2012 NSUSY fits *J. High Energy Phys.* JHEP12(2012)077
[10] Ellis J, Murphy C W, Sanz V and You T 2018 Updated global SMEFT fit to Higgs, Diboson and electroweak data *J. High Energy Phys.* JHEP06(2018)146
[11] CMS Collaboration 2020 Search for top squark pair production using dilepton final states in pp collision data collected at $s = 13$ TeV (arXiv:2008.05936)
[12] ATLAS Collaboration 2018 Search for top-squark pair production in final states with one lepton, jets, and missing transverse momentum using 36 fb^{-1} of $s = 13$ TeV pp collision data with the ATLAS detector *J. High Energy Phys.* JHEP06(2018)108
[13] Budge L, Campbell J M, De Laurentis G, Ellis R K and Seth S 2020 The one-loop amplitudes for Higgs + 4 partons with full mass effects (arXiv:2002.04018)
[14] Dawson S, Djouadi A and Spira M 1996 QCD corrections to supersymmetric Higgs boson production: the role of squark loops *Phys. Rev. Lett.* **77** 16
[15] Gunion J F and Haber H E 2003 The CP conserving two Higgs doublet model: the approach to the decoupling limit *Phys. Rev.* D **67** 075019
[16] Britto R, Cachazo F and Feng B 2005 Generalized unitarity and one-loop amplitudes in super-Yang–Mills *Nucl. Phys.* B **725** 275
[17] Forde D 2007 Direct extraction of one-loop integral coefficients *Phys. Rev.* D **75** 125019
[18] Mastrolia P 2009 Double-cut of scattering amplitudes and Stokes theorem *Phys. Lett.* B **678** 246
[19] Kilgore W B 2007 One-loop integral coefficients from generalized unitarity (arXiv:0711.5015)
[20] Davies S 2011 One-loop QCD and Higgs to partons processes using six-dimensional helicity and generalized unitarity *Phys. Rev.* D **84** 094016
[21] Hodges A 2013 Eliminating spurious poles from gauge-theoretic amplitudes *J. High Energy Phys.* JHEP05(2013)135
[22] Badger S, Frellesvig H and Zhang Y 2013 A two-loop five-gluon helicity amplitude in QCD *J. High Energy Phys.* JHEP12(2013)045
[23] Badger S 2016 Automating QCD amplitudes with on-shell methods *J. Phys.: Conf. Ser.* **762** 012057
[24] Hartanto H B, Badger S, Bronnum-Hansen C and Peraro T 2019 A numerical evaluation of planar two-loop helicity amplitudes for a W-boson plus four partons *J. High Energy Phys.* JHEP09(2019)119
[25] de Laurentis G and Maître D 2019 Extracting analytical one-loop amplitudes from numerical evaluations *J. High Energy Phys.* JHEP07(2019)123
[26] Harland-Lang L, Martin A, Motylinski P and Thorne R 2015 Parton distributions in the LHC era: MMHT 2014 PDFs *Eur. Phys. J.* C **75** 204
[27] Cohen T, Majewski S, Ostdiek B and Zheng P 2020 On the ATLAS top mass measurements and the potential for stealth stop contamination *J. High Energy Phys.* JHEP06(2020)019
[28] Greiner N, Höche S, Luisoni G, Schönherr M and Winter J-C 2017 Full mass dependence in Higgs boson production in association with jets at the LHC and FCC *J. High Energy Phys.* JHEP01(2017)091
[29] Chen X, Gehrmann T, Glover E W N and Jaquier M 2015 Precise QCD predictions for the production of Higgs + jet final states *Phys. Lett.* B **740** 147
[30] Chen X, Cruz-Martinez J, Gehrmann T, Glover E W N and Jaquier M 2016 NNLO QCD corrections to Higgs boson production at large transverse momentum *J. High Energy Phys.* JHEP10(2016)066
[31] Bizon W *et al* 2018 Fiducial distributions in Higgs and Drell-Yan production at $\text{N}^3\text{LL} + \text{NNLO}$ *J. High Energy Phys.* JHEP12(2018)132
[32] Boughezal R, Caola F, Melnikov K, Petriello F and Schulze M 2015 Higgs boson production in association with a jet at next-to-next-to-leading order *Phys. Rev. Lett.* **115** 082003
[33] Campbell J M, Ellis R K and Seth S 2019 $H + 1$ jet production revisited *J. High Energy Phys.* JHEP10(2019)136
[34] Del Duca V, Kilgore W, Oleari C, Schmidt C and Zeppenfeld D 2001 Gluon-fusion contributions to $H + 2$ jet production *Nucl. Phys.* B **616** 367